crystals

MDPI

Article

Self-Polarization in $PbTiO_3$ Crystals Induced by Chemical Inhomogeneity in the Surface Layer

Vladimir A. Stephanovich [1], Christian Rodenbücher [2], Michal Pilch [3], Jacek Szade [3,†], Andrzej Molak [3], Gustav Bihlmayer [4,*] and Krzysztof Szot [3,5]

[1] Institute of Physics, Opole University, Oleska 48, 45-052 Opole, Poland; stef@uni.opole.pl
[2] Forschungszentrum Jülich GmbH, Institute of Energy and Climate Research (IEK-14), 52425 Jülich, Germany; c.rodenbuecher@fz-juelich.de
[3] August Chełkowski Institute of Physics, University of Silesia in Katowice, ul. 75 Pułku Piechoty 1, 41-500 Chorzów, Poland; michal.pilch@us.edu.pl (M.P.); andrzej.molak@us.edu.pl (A.M.); krzysztof.szot@us.edu.pl (K.S.)
[4] Peter Grünberg Institut and Institute for Advanced Simulation, Forschungszentrum Jülich and JARA, 52425 Jülich, Germany
[5] aixACCT Systems GmbH, 52068 Aachen, Germany
* Correspondence: g.bihlmayer@fz-juelich.de
† Deceased.

Abstract: We study the so-called self-polarization phenomenon in single, electroded $PbTiO_3$ crystals. In this case, near the electrodes, surface layers are formed with a chemically modified perovskite structure. This generates a built-in electric polarization, which cannot be switched permanently by an external electric field. While the initial samples, having two such surface layers with opposite directions of built-in polarization, exhibit ordinary symmetric hysteresis loops, the "asymmetric" samples, with one of these surface layers removed, show asymmetric hysteresis loops. To describe our experimental findings, we combine two kinds of models: one is phenomenological, utilizing the above general features; and the other is ab initio, taking into account the actual atomic structure at the bulk ferroelectric–surface layer–electrode interface. Namely, the ab initio calculations show that the electric polarization within the surface layer occurs due to the shifts of the relaxed Ti ions with respect to the oxygen ion octahedra on the PbO-terminated surface. We ascribe the self-polarization effect to the occurrence of the built-in electric field resulting from the formation of Pb-O planes within the surface layer.

Keywords: lead titanate; hysteresis loops; surface layer; ferroelectrics

check for updates

Citation: Stephanovich, V.A.; Rodenbücher, C.; Pilch, M.; Szade, J.; Molak, A.; Bihlmayer, G.; Szot, K. Self-Polarization in $PbTiO_3$ Crystals Induced by Chemical Inhomogeneity in the Surface Layer. *Crystals* **2023**, *13*, 1155. https://doi.org/10.3390/cryst13081155

Academic Editor: Zhilun Lu

Received: 27 June 2023
Revised: 17 July 2023
Accepted: 19 July 2023
Published: 25 July 2023

1. Introduction

Several attempts have been made to explain some physical effects in ferroelectric (FE) perovskites by assuming that the properties of the surface layer differ from those of the bulk. Namely, that such features as the dielectric permittivity, electrical conductance, optical absorption, and domain wall (DW) properties [1–3] would be different. The latter properties of ferroelectrics, which are determined by the interaction between the bulk and the surface layer contributions, have been intensively studied. These are also affected by the extrinsic effects related to the homogeneous or the inhomogeneous chemical composition, the presence of impurities or doping [4–7], structural defects, the strain–stress effect, as well as the electric polarization variance [8–10]. Hence, it is a challenge to determine to what extent manipulation of the physical and chemical features of the surface layer may lead to the tuning of the electrical properties of the surface and bulk. The functional goals to be considered are related to the stability and the switching conditions of the polarization perpendicular to the surface of the FE material. A stable orientation can be obtained in a several nm thin layer, as has been shown by calculations [11,12] and proved by experiments [13,14]. The standard procedure used for the formation of an FE polarization is based on the reorientation of the FE domains, induced by the application of external electric fields that are higher than the coercive field or by a suitable combination of mechanical stress and temperature gradient at the paraelectric (PE)–FE phase transition. In cases where the poling occurs at a temperature higher than the PE–FE phase transition temperature, this may be accompanied by electronic or ionic leakage currents. However, the ionic current may lead to side effects, such as the rearrangement of the structure within the formed material. The conditions for the controlled stabilization and switching of the FE polarization are still being studied and discussed [2,9,15–19].

Most of the models of the self-polarization effect in FE materials have been developed for thin films, whose geometrical configuration is, per se, asymmetrical (i.e., a substrate with deposited thin films [20]), and, therefore, cannot be applied automatically to a single crystal, which represents a self-supported structure with full symmetric boundary conditions. In fact, for a virgin $PbTiO_3$ crystal, one can observe a perfect hysteresis loop without a so-called imprint [21]. This compound is still the basis for applications where large polarization effects are needed [22,23] and its use ranges from memories to energy materials [24,25]. The goal of our paper is to explain what kind of treatment of a virgin $PbTiO_3$ single crystal (with perfect FE properties), without electrical poling, allows the creation of a system with a distinguished direction of polarization. We will reach this effect by applying a combination of controlled thermodynamic procedures (here moderate temperature of 600 °C and high activity of oxygen) in order to induce structural and chemical modifications in the surface layer. In this way it is possible to produce a stabilized non-zero net P_S in $PbTiO_3$ crystals without the preliminary application of an external electric field. Alternatively, this state can be obtained by applying the unbalanced contributions from the chemically modified surface layer.

We suggest that the chemically modified surface layer on $PbTiO_3$ can be formed by thermal treatment of a single crystal under oxidizing conditions (similar to [2,7,26,27]). Thermal annealing conducted in conditions different from those used for the crystal growth ought to lead to the outward migration of ions. Such chemically inhomogeneous structures may form an electronic or ionic space charge within the surface layer. Consecutively, polarization can be induced within the surface layer. Its orientation is expected to be perpendicular to the surface of the perovskite material. The polarization would be stable since the inhomogeneous chemical effects are frozen yet at a moderate temperature range. Hence, the produced perpendicular alignment of the FE polarization ought to be fixed or resistant to external fields.

The above effects can be described within the so-called self-polarization model. The concept of self-polarization is not new; this scenario had been used about twenty years ago to describe the fact that a significant amount of polarization exists in virgin synthesized bulk material without pre-poling treatment [28]. Self-polarization has been observed in thin ferroelectric films (especially for $PbTiO_3$ and $Pb(Zr_xTi_{1-x})O_3$ (PZT)) prepared by different deposition methods (see, e.g., [29–33]). A stable self-polarization effect can be obtained in $PbTiO_3$ in a wide temperature range due to the fact that the FE–PE phase transition occurs at a high temperature of around 490 °C–493 °C [34]. Moreover, the spontaneous polarization, P_S, estimated from the ionic shifts, has a high value 0.73–0.81 C m^{-2} [10,34,35]. Comparable magnitudes (P_S = 0.80 C m^{-2} [36,37]) can be obtained from standard pyroelectric and P–E hysteresis loop measurements [15]. The FE order in the $PbTiO_3$ crystals has been observed in the perovskite phase with tetragonal symmetry and unit cell parameters a = 3.900 Å and c = 4.150 Å (tetragonality c/a = 1.064) at room temperature [38].

It has been shown by ab initio calculations, that the spontaneous polarization switching in the thin $PbTiO_3$ layer is affected by the termination of the crystal structure. This means that both PbO-terminated and TiO_2-terminated surfaces ought to be considered. Moreover, the oxygen vacancy, V_O, defects also affect the electronic structure, the P_S value and its switching characteristics [6,15,39]. One can notice a correlation between the thermally treated $PbTiO_3$ crystals and the Ruddlesden–Popper (RP) structure that shows a close analogy to the perovskite matrix phase and simultaneously has a stoichiometry shifted towards the AO excess in a layered AO–$(ABO_3)_n$ (n = 1, 2, 3, . . ., ∞) structure. In thermally treated $PbTiO_{3-x}$ single crystals, $PbO(PbTiO_3)_n$ phases with n = 1–10 and a lattice parameter similar to $PbTiO_3$ have been identified [40].

The aim of this work is to confirm whether it is possible to induce self-polarization in the surface of the FE $PbTiO_3$. For that, we use different experimental techniques, assisted by ab initio and phenomenological theoretical modeling: FE hysteresis loop studies, measurements of the electromotive force's temperature dependence and thermo-stimulated currents as well as piezoresponse force microscopy (PFM) images. The combination of the above techniques enables us to discern the contributions from the surface layer and from the bulk.

2. Materials and Methods

2.1. Crystal Growth and Characterization

We have used single crystals grown by the flux method (for details, see ref. [41–43]). This method was described earlier by Fesenko [44]. The transparent crystals chosen for the experiment were in the form of rectangular plates and exhibited a low electric conductivity of the order of 10^{-11} S cm^{-1} at room temperature. The ferroelectric domain patterns were observed with the use of a polarizing microscope.

Three series of samples were prepared. The virgin, as-grown crystal samples were prepared for electrical tests. The as-grown and cleaved samples were taken for the atomic force microscopy (AFM) and PFM tests. The third series of the samples were treated at high temperature for several hours (e.g., 10, 12, 15 h) under oxidizing conditions at $p(O_2)$ = 200 Torr. Some samples were tested directly after this treatment, whereas others were cleaved prior to the tests.

The crystal samples, their symmetry, and phase content were first characterized by X-ray diffraction (XRD) tests (see, e.g., [40]). The results for virgin (as-grown) and oxidized crystal were published in an earlier paper [41].

2.2. AFM/PFM Tests

The atomic force microscope JEOL 4210A equipped with Pt/Ir conducting tips (Nanoworld) operating in the contact mode was applied. A DC voltage source and femtoammeter setup was used to measure the electrical local conduction (LC-AFM). The measurement was conducted for the virgin cleaved crystal and for the crystal oxidized at 650 °C for 12 h. The topography images and the piezoresponse of the crystal surface were recorded at room temperature and ambient air at a pressure lowered to ~5×10^{-8} bar. The WinSPM program (Scanning Probe Microscopes, JEOL) was applied. The piezoelectric response (PFM) measurement was carried out using the atomic force microscope described above. The PFM signal, obtained in the contact mode, was amplified with two lock-in voltmeters, separately for the in-plane and out-of-plane orientations.

2.3. Electrical Measurements

Rectangular samples with a thickness $d \approx 0.1$ mm and painted with Ag paste were prepared. Two different configurations of the samples, i.e., "symmetric" and "asymmetric", were prepared in order to verify the influence of the surface layer features on the effective macroscopic electric properties of lead titanate crystals.

The "symmetric configuration" corresponds to the virgin sample consisting of the perovskite bulk wrapped up in the surface layer, and formed in the growth process (Figure 1a, see also Figure 2a for a more detailed view). The surface layer was also purposefully modified due to the reaction with ambient air during high temperature treatment (Figures 1b and 2b). The electrodes were placed on the surface layers, and the sequence "electrode–surface layer–bulk–surface layer–electrode" was obtained for both cases (see Figures 1a,b and 2a,b). The "asymmetric" configuration of the sample (Figures 1c and 2c) was obtained after removing the surface layer, produced at high temperatures. This was achieved either by polishing only one side of the crystal sample with diamond paste or by cleaving the sample. After this procedure, the electrodes were deposited. Hence, the sequence "electrode–bulk–surface layer–electrode" could be produced.

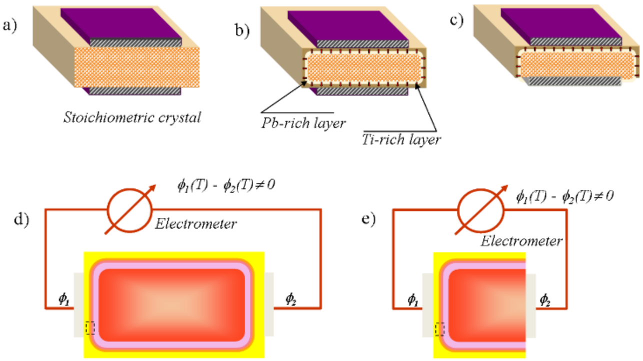

Figure 1. The "symmetric" (**a**,**b**) and "asymmetric" (**c**) configurations of the $PbTiO_3$ crystal samples prepared for the electrical measurements (thermo-stimulated current, *I*–*E* hysteresis loop). The "symmetric" (**d**) and "asymmetric" configurations (**e**) samples are used for electromotive force measurement.

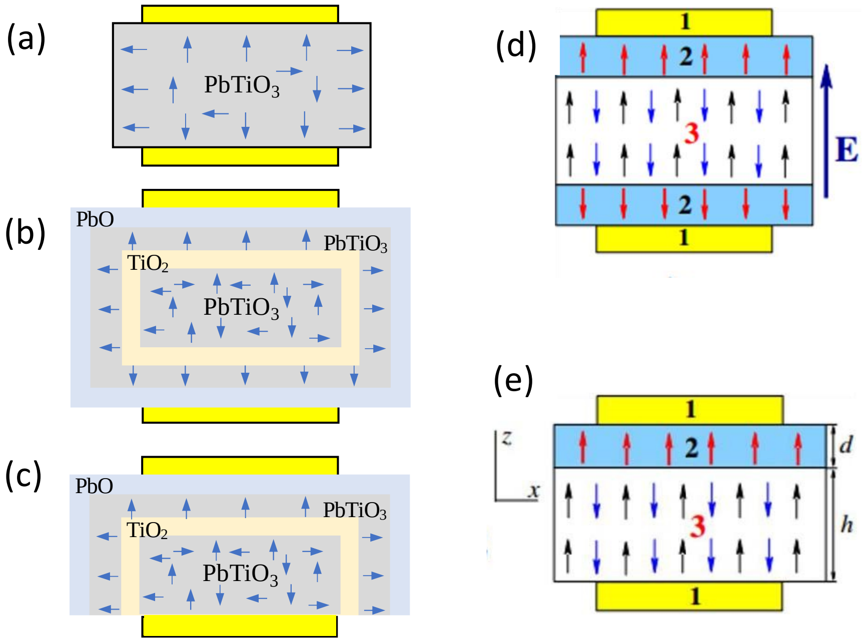

Figure 2. Diagrams showing a model of the surface layer structure. (**a**) The chaotic set of FE domains in ABO_3 bulk in the as-grown sample. (**b**) Scheme of the multi-component surface layer enveloping the ABO_3 bulk after the thermal treatment. (**c**) One electrode placed on the surface layer, the second deposited directly on the unwrapped bulk, after the sample was cleaved. Panels (**d**,**e**) show the sketch of the above structure, adopted for model theoretical calculations. Region 1—electrodes, region 2—self-polarized layer (of thickness d) with built-in polarization (bold red arrows), and region 3—ferroelectric of thickness h. Panel (**d**) reports the symmetric structure with opposite directions of built-in polarization in the upper and lower self-polarized layers. Here, the opposite polarization directions (black and blue arrows) in FE layer are compensated by those in layers 2, generating a symmetric hysteresis loop. Panel (**e**) shows the non-symmetric structure, obtained by cutting the sample apart (in contrast to panel d). Thus, one of the polarization directions (blue arrows in this case) in the FE layer 3 is not compensated, creating an energetically unfavorable "tail-to-tail" configuration with built-in polarization of layer 2, which produces asymmetry of the hysteresis loop. The local reference frame and direction of the external electric field E are also shown.

The thermo-stimulated currents (TSCs) were recorded at a constant rate of temperature increase dT/dt = 0.1 K s^{-1} in the vicinity of the FE phase transition, $T_C \approx 490$ °C. The TSC from the $PbTiO_3$ single crystal samples was obtained for: (a) a virgin stoichiometric crystal, (b) a crystal after thermal treatment at oxidizing conditions in the paraelectric phase, and (c) a crystal which has been prepared as in point (b), but with the surface layer removed from one side to obtain an “asymmetric configuration”. Although the samples were not polarized prior to the measurement, in the thermo-stimulated current, contributions from the pyroelectric current should be observed [29,45]. The electric current–electric field (*I*–*E*) hysteresis loop [1,46] measurement was performed on the multi-domain crystals both for the “symmetric” as well as the “asymmetric” cases. A triangular voltage sweep at frequency f = 0.01 Hz and strength up to 25 kV cm^{-1} was applied using a triangular signal generator and a digital oscilloscope for recording. The value of the remnant polarization was estimated from these *I*–*E* loops.

The temperature dependence of the electromotive force (EMF) was measured with the use of an electrometer (6430-Keithley). The crystal sample was prepared as follows: the $PbTiO_3$ sample was oxidized at 650 °C, cleaved to obtain an “asymmetric configuration” (Figures 1e and 2c), and then the electrodes were deposited. In this case, one electrode was deposited on the sample’s surface layer. The other electrode was deposited directly on the bulk after cleaving. The measurement was carried out within the FE phase during heating to a range of ~200–460 °C. The analog electrical data for the hysteresis loop measurements were collected using a system Adwin-Gold (Jäger).

2.4. EDX Investigation

For the compositional analysis of the surface layer of an oxidized $PbTiO_3$ crystal at the nanoscale, electron dispersion X-ray spectroscopy (EDX-Oxford Instruments ISIS300, SiLi detector with an ultrathin window), combined with an analytical TEM (Philips CM 200, LaB6 cathode, 200 kV), was performed on small particles taken from the surface of a single crystal.

2.5. Calculations

Here we perform two kinds of calculations, ab initio and model. The ab initio calculations were performed using density functional theory (DFT) in the generalized gradient approximation (GGA) proposed by Wu and Cohen [47]. The full-potential linearized augmented plane-wave (LAPW) method [48] was used.

A general theoretical approach to the description of the layered dielectric structures, especially those containing ferroelectric layers, consists in the application of the coupled system of Ginzburg–Landau equations for the ferroelectric layers and Maxwell equations for passive (paraelectric or other non-ferroelectric) layers, augmented by corresponding boundary conditions at the interfaces. All of the above equations contain phenomenological material parameters such as dielectric permittivity, which in such general case is frequency and thickness dependent. The resulting complicated equation of state [49–51] contains not only the polarization (both spontaneous in ferroelectric and induced in non-ferroelectric layers) but also its spatial derivatives. This requires more boundary conditions [52,53], severely complicating the situation and, because the analytical solution of the above set of equations in the general case is impossible and the numerical solution (the so-called phase-field method, see ref. [54] and references therein) is computationally extremely intensive, requiring some model considerations. Therefore, in problems of multilayer structures, researchers usually resort to the model calculations, which capture the essential physics (and sometimes even can give a quantitative description of the experiments) surprisingly well [49,50,55,56]. For instance, for sufficiently thin layers, the corresponding boundary conditions can serve as the equation of state (i.e., the equation relating the internal electric field and polarization, [49]) in both blocking and ferroelectric layers. Our subsequent calculations show that such very simple description gives a fairly good coincidence with the experiment.

In our model calculations, we consider a $PbTiO_3$ layer with built-in polarization (so-called self-polarized layer), which exists at the interface between the FE (also $PbTiO_3$) layer and the electrode, and that is nonconductive. The latter means that the built-in polarization sustains for a long time. In our model, this polarization cannot be switched by the application of an external electric field. In order to satisfy the continuity of the electric displacement vector, D, and the electric field, E, at the interface, the polarizations of FE and self-polarized layers form "head-to-tail" or "tail-to-head" configurations, as illustrated in the Figure 2d. When the polarization in the FE layer switches its direction by application of a voltage, the self-polarized layers turn to a state with a discontinuity of the polarization, termed a "head-to-head" or "tail-to-tail" structure. The discontinuity of the polarization generates a strong electric field. After removal of external voltage, this field works to switch the FE polarization back to the "up" state to restore the continuity. In Figure 2d, this process is shown to generate the ordinary symmetric hysteresis loop as the built-in polarizations in the upper and lower layers have opposite directions. This is not the case in Figure 2e, where one of the polarization directions in the ferroelectric layer is not compensated by a corresponding built-in polarization. As we shall see below, this generates an asymmetric hysteresis loop.

3. Results

3.1. Piezoresponse in Nanoscale

The multi-domain state of the $PbTiO_3$ crystals was confirmed with the polarizing microscope test. The rectangular array of the domains indicated the possibility of compensation of the FE domain contribution to the net electric polarization (Figure 3).

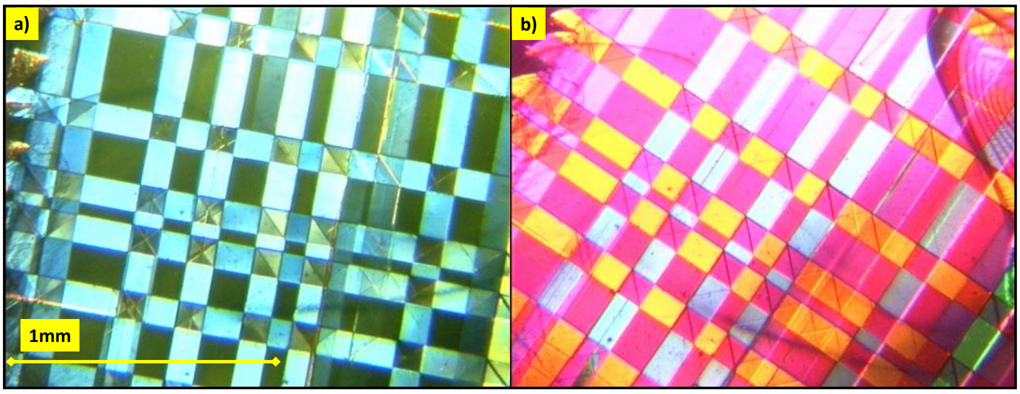

Figure 3. Panels (**a**,**b**) show examples of "*a*" and "*c*" domain patterns, respectively, in a $(100)_{pc}$-plate of an as-grown tetragonal $PbTiO_3$ single crystal. The image was obtained by a polarization microscope.

The occurrence of the FE domains was tested at the nanoscale by piezoresponse measurements (PFM). Although the polarizing microscope studies show a rectangular network of domains on the nanoscale PFM images (Figure 4), the DWs (in-plane and out-of-plane) are more rounded and not as sharply defined. This effect can be ascribed to the influence of the strong electric field on the DWs, probably resulting from structural defects. Nevertheless, the FE domains remained in the $PbTiO_3$ crystals, though their shapes were affected.

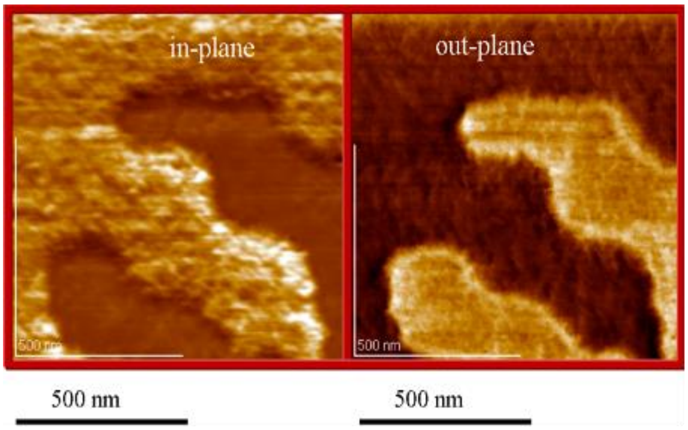

Figure 4. Examples of the arrangements of "*a*" and "*c*" domains in a $(100)_{pc}$-plate of tetragonal $PbTiO_3$ single as-grown crystal. The images were obtained using a PFM for both the in-plane (**left**) and the out-of-plane (**right**) mode.

The search for the origin of self-polarization induced by oxidation of the $PbTiO_3$ crystal calls for an investigation of the surface's FE (piezoelectric) properties, where the morphology has been dramatically modified during oxidation. After the recrystalization induced by oxidation, the surface of the crystal is covered with many crystalites (see Figure 5a and ref. [57]). PFM on such a rough surface shows a high lateral inhomogeneity (see Figure 5b,c). One can observe an anticorrelation between areas with high piezoelectric response and regions with good electrical conductivity (Figure 5b–d).

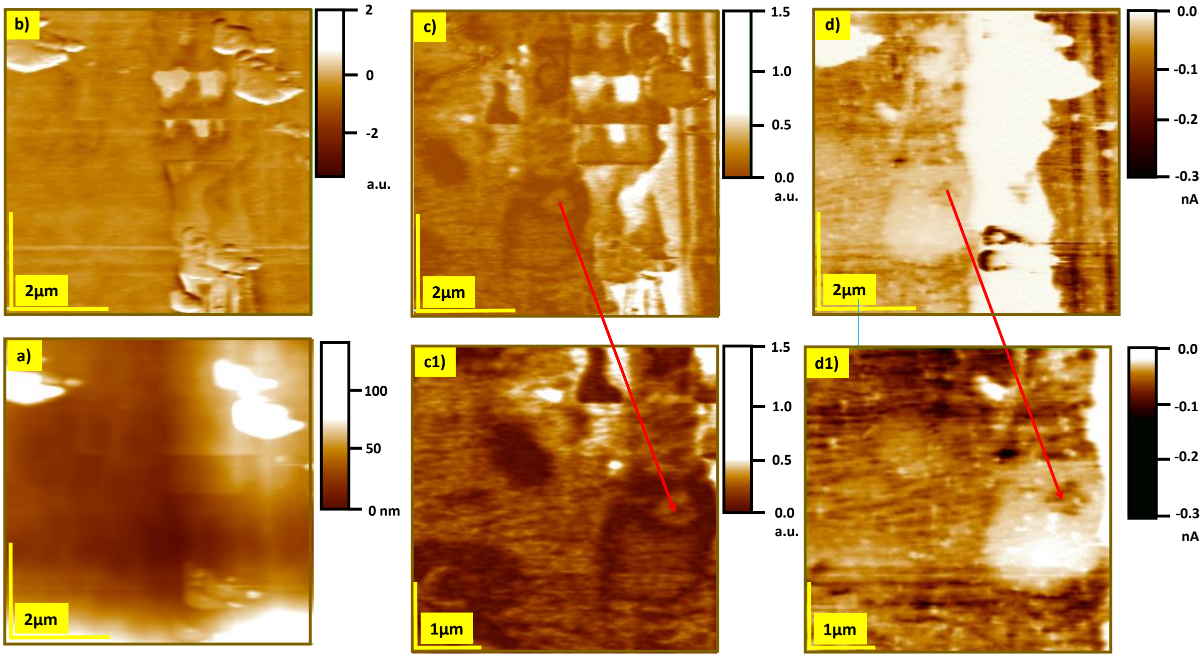

Figure 5. Topography (**a**), piezoresponse in-plane (**b**) and out-of-plane (**c**,**c1**), and local conductivity maps (**d**,**d1**) of a $PbTiO_3$ crystal oxidized at 650 °C. Magnification of the out-of-plane piezoresponse (**c1**) depicts a stripe-like nanodomain. The magnification of the electrical conductivity image (**d1**) shows a linear arrangement of the conducting filaments in the same region. Because water contamination can dramatically reduce the amplitude of PFM and current flow, the measurement was obtained in a high vacuum at 250 °C in order to desorb water molecules from the surface.

LCAFM measurements performed at 250 °C on an oxidized $PbTiO_3$ crystal reveal that the conductivity is filamentary and can vary by several orders of magnitude between the filaments and the matrix. The band arrangement observed for the conducting filaments (see Figure 5(d1)) also occurs in the piezoresponse. This form of piezoelectric arrangement may be connected with the creation of $PbO(PbTiO_3)_n$ (Ruddlesden–Popper phases with high n) as the growth of these phases in the upper part of the surface region during oxidation has been proven for different perovskites ($BaTiO_3$, $SrTiO_3$, $PbTiO_3$, $KnbO_3$) with roentgenographic studies [40].

3.2. Electric Polarization

The thermo-stimulated currents were measured both on the as-grown and the thermally treated samples. The obtained results are shown in Figure 6. In the case of the virgin, as-grown, $PbTiO_3$, the sample was in the "symmetric configuration", and it was not polarized by an external field prior to the measurement. Hence, the expected and most probable net "natural" polarization was equal to zero due to its compensation in the FE domains. Therefore, the current peaks in the vicinity of the FE–PE transition (Figure 6a) can be classified as Barkhausen noise.

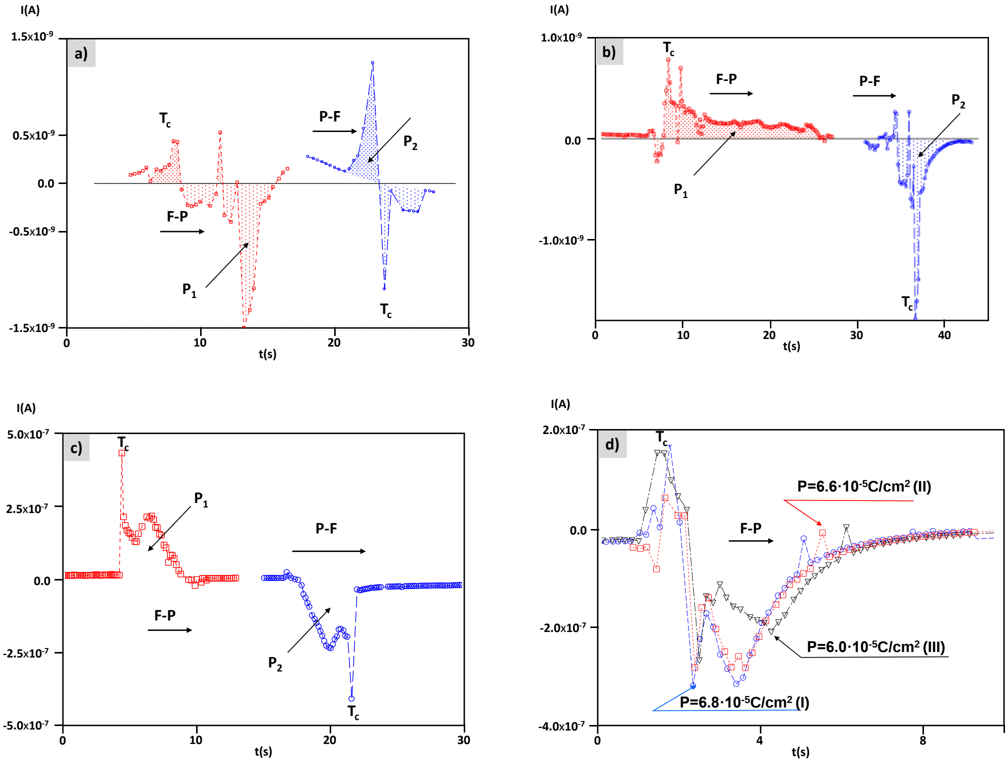

Figure 6. TSC as a function of time in $PbTiO_3$ single crystals recorded for FE–PE (F–P, depolarization current induced by heating) and for PE = FE transitions (P–F, polarization current induced by cooling): (**a**) virgin stoichiometric crystal, (**b**) crystal after thermal treatment (oxidized in para-phase) when the chemically inhomogeneous surface layer covers the whole crystal ("symmetric configuration"). The current is measured when a crystal has been prepared in an "asymmetric" configuration case, i.e., with a surface layer removed on one side of the crystal, identified as the "pyro-electric current" is shown in (**c**). The persistence of the self-polarization effect can be observed in an asymmetric system by repeated heating through the phase transition; in this case, the polarization values are very similar to the polarization measured in the first heating cycle (**d**). The net polarization determined after integration of the TSDC is: $P_1 = 9 \times 10^{-4}$ C m^{-2}, $P_2 = 6 \times 10^{-4}$ C m^{-2} for the virgin crystal (**a**); $P_1 = 3 \times 10^{-3}$ C m^{-2}, $P_2 = 3 \times 10^{-3}$ C m^{-2} for the oxidized crystal in symmetric configuration (**b**); $P_1 = 0.7$ C m^{-2}, $P_2 = 0.76$ C m^{-2} for the oxidized crystal in asymmetric configuration (**c**); and $P_{I} = 0.68$ C m^{-2}, $P_{II} = 0.66$ C m^{-2}, and $P_{III} = 0.60$ C m^{-2} for the repeated measurements (**d**).

The current measured in a sample that had been thermally treated within the PE phase (T = 650 °C) in ambient air, is shown in Figure 6b. A flat and narrow anomaly can be discerned, within experimental accuracy, in the vicinity of the FE–PE phase transition. The oxidizing conditions provided effective chemical gradients in the high temperature range, which in turn may have caused the migration of ions from the bulk towards the surface and have resulted in a chemical modification of the surface layer. One can expect that such a deliberately modified layer might affect the properties of the sample. However, the lack of a marked peak in the measured current/temperature dependence would correspond with the compensated net electric polarization. However, an unexpected result occurred when the preliminarily unpolarized crystalline $PbTiO_3$ sample was prepared in the "asymmetric" configuration. A substantial current peak appears in the vicinity of the FE–PE phase transition temperature, exhibiting a maximum at 496 °C (Figure 6c). The magnitude of the polarization estimated by integration was 0.7 C m^{-2}. The latter peak might either originate from a defect-generated space charge or from the charge density variation due to FE phase transition. If the effect is related to the deep level traps, introduced by the applied thermal treatment, then it should occur both for the "symmetric" and the "asymmetric" configuration of the samples. As this is not the case, another explanation is proposed. Namely, the mechanical removal of the modified surface layer from only one side of the sample to expose the natural polarization of the bulk to direct contact with the re-deposited electrode. We interpret the occurrence of the peak in Figure 6c as the manifestation of the FE–PE phase transition, because the charge density changes when the spontaneous polarization vanishes. During cooling, an opposite current of similar magnitude appears when the sample goes through the PE–FE phase transition. Hence, the electric polarization of the sample is not compensated macroscopically in the "asymmetric" configuration. This allows us to deduce that the lack of the net polarization compensation is related to the modified surface layer. Moreover, one can consider the observed peak as the pyroelectric current peak [35].

The electric current–electric field (*I*–*E*) hysteresis loops recorded for samples of the as-grown crystal and the crystals after oxidation (in the "symmetric" and "asymmetric" configuration) are shown in Figure 7. The measurement of the as-grown sample shows the symmetric *I*–*E* hysteresis loop (Figure 7a) under the application of the triangular periodic electric field pulses. The spontaneous polarization estimated from both *I*–*E* loop branches, labeled "+" and "−", are similar in absolute value: $P_+ = 0.84$ C m^{-2} and $P_- = -0.80$ C m^{-2}. This yields values that are comparable to the one reported in the literature i.e., $P_S = 0.80$ C m^{-2} [35–38]. The coercive field equals $E_C = 2.6$ kV cm^{-1}. The similarity of P_+ and P_- is compatible with the spatial features of this sample as the virgin sample consists of the bulk FE perovskite lattice enveloped or wrapped uniformly by a surface layer formed during the growth process. One can notice that the estimated P_S value is comparable to that obtained/calculated from the XRD data. Hence, in this case the surface layer contribution is insignificant.

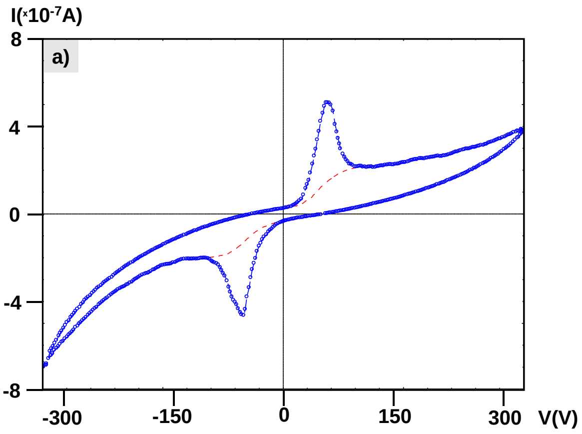

Figure 7. *Cont.*

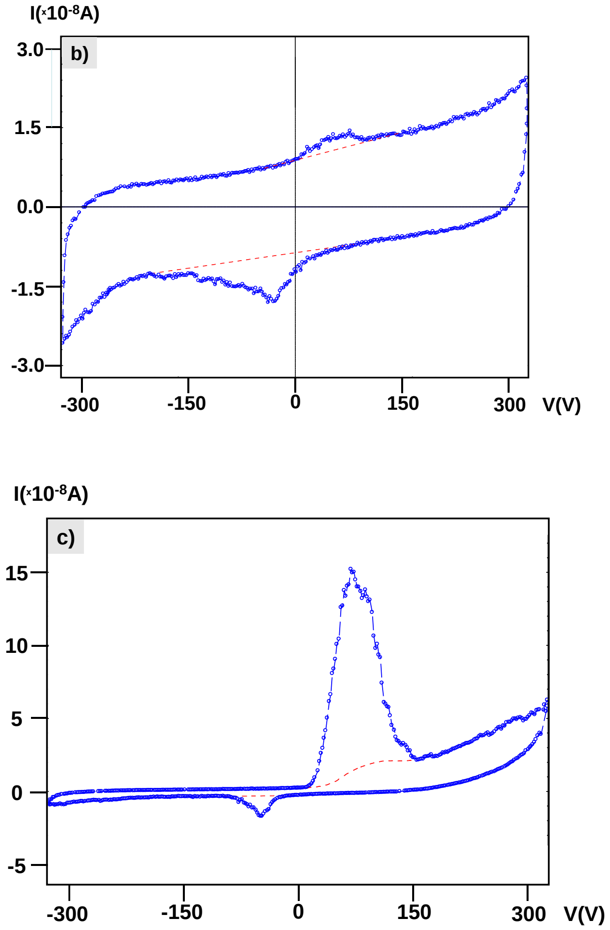

Figure 7. (**a**) I/V hysteresis loop of a virgin (as-grown) $PbTiO_3$ single crystal. Polarization triangle voltage sweep (TVS) f = 0.001 Hz, T = 300 °C, p_{O2} = 200 mbar, thickness d = 0.2 mm, Ag electrode. The dotted red line indicates the standard non-ferroelectric background used for the polarization analysis. $P_+ = 0.84$ C m^{-2}, $P_- = -0.80$ C m^{-2}, E_{c+} = 2.6 kV/cm, $E_{c-} = -2.6$ kV/cm; (**b**) as above for an oxidized $PbTiO_3$ single crystal in symmetric configuration, TVS: f = 0.001 Hz, T = 300 °C, p_{O2} = 200 mbar, thickness d = 0.2 mm, electrode: Ag. $P_+ = 0.003$ C m^{-2}, $P_- = -0.014$ C m^{-2}, E_{c+} = 3.1 kV/cm, $E_{c-} = -1.9$ kV/cm; (**c**) as above for an oxidized $PbTiO_3$ single crystal in the asymmetric configuration, TVS: f = 0.001 Hz, T = 300 °C, p_{O2} = 200 mbar, thickness d = 0.19 mm, electrode: Ag. $P_+ = 0.86$ C m^{-2}, $P_- = -0.032$ C m^{-2}, E_{c+} = 3.5 kV/cm, $E_{c-} = -2.3$ kV/cm.

The sample that had been treated at high temperatures exhibited a diminished and slightly asymmetric *I*–*E* hysteresis loop (Figure 7b). The estimated values of polarization were equal to $P_+ = 0.003$ C m^{-2} and $P_- = -0.014$ C m^{-2}. Moreover, a rise in the leakage current was observed when the applied electric field was increased.

The *I*–*E* hysteresis loops obtained both for as-grown and oxidized crystals in symmetric configuration (shown in Figure 7a,b) yield similar values of P_+ and P_-, which coincides with the pyroelectric current measurements (compare Figure 7a,b to Figure 6a,b). However, the P_S value, obtained for the as-grown (a) and thermally treated (b) samples, differs by about one order of magnitude. In the case of the as-grown sample the charge bound by the FE bulk was released and measured. In case (b), after thermal treatment of the sample, a decreased value of P_S occurred. We ascribe this effect to the surface layer formed by ionic migration. Such a migration is possible in a high temperature range where the chemical gradients are effective. Therefore, the modified surface layer, which was chemically disturbed and different from the FE bulk, dominated the actual polarization estimated for the multi-component sample. This assumption is supported by results obtained by secondary-ion mass spectrometry (SIMS) results, which are presented in detail below, and by the results obtained in an earlier work [41], where it was shown that the Ruddlesden–Popper phases $PbO(PbTiO_3)_n$, (n = 1, 2, 3, 4, 5, 6) were formed on the $PbTiO_3$ crystal surface after similar thermal treatment.

The *I–E* hysteresis loop for the "asymmetric sample" (c), obtained after the removal of surface layer from one side of the crystal (see Figures 1c and 2c), is shown in Figure 7c. In effect, the asymmetry was induced by depositing one electrode directly onto the $PbTiO_3$ bulk. The actual values of P_+ and P_- were estimated as 0.86 C m^{-2} and −0.032 C $m^{-2,}$ respectively. The coercive field values are E_{c+} = 3.5 kV cm^{-1} and E_{c-} = −2.3 kV cm^{-1}.

Hence, the properties of sample (c) can be described as a superposition of the properties of samples (a) and (b). For the as-grown ABO_3 sample (a), one has a chaotic set of FE domains (Figure 2a). This makes the P_S reorientation possible so that the proper *I–E* hysteresis loop occurs. In contrast, for sample (b), the P_S can only be fixed partially when the segregation of oxides appears in the surface layer. Moreover, the applied external field was varied up to $E_{EXT} = \pm 25$ kV cm ^{1}, i.e., it was much higher than the corresponding coercive fields E_C. We have found that the "surface layer" electric field $E_{SL} > E_C$ develops and establishes within the surface layer as a consequence of the ionic migration forced by the thermal treatment. Hence, E_{SL} can essentially block the polarization reorientation on one side of the sample. This is manifested by the diminished values of the measured, effective polarization P_- which is equal to 0.03 C m^{-2} (see Figure 7c).

3.3. Electromotive Force ϵ (T)

The measurement of the electromotive force, $\epsilon(T)$, was conducted both for the oxidized "symmetric" sample (Figure 1b) and the oxidized "asymmetric" sample (Figure 1c). A lack of electromotive force $\epsilon(T)$ was observed for the "symmetric" sample. In contrast, the "asymmetric" sample produced a pronounced $\epsilon(T)$ signal dependent on temperature, $d\epsilon(T)/dT > 0$ (Figure 8). We propose to ascribe a linear $\epsilon(T)$ = A + BT dependence to the variance in the Pb^{2+}/Pb^0 ratio (see XPS data below) within the surface layer of the $PbTiO_3$ crystal. We would like to emphasize that the measured signal was not related to the Seebeck effect, as the temperatures of the sample and the electrodes $T_{el,1} = T_{\text{sample}} = T_{el,2}$ were equal to each other. Therefore, we assume that $\epsilon(T)$ originates from the chemically inhomogeneous surface layer. The gradient $d\epsilon(T)/dL$ can be estimated. Because the $\epsilon(T)$ varies from 0.15 V to 0.25 V and the surface layer depth (taken from the SIMS test) is ~20 nm for the Pb-rich layer and/or ~50 nm for the whole Pb–Ti surface layer, we calculated the gradient value to be $d\epsilon(T)/dL \approx 10^5$ V cm^{-1}. The estimated electromotive force gradient was at least one order of magnitude higher than the coercive field E_C~10^3 V/cm. Hence, such a strong field, locked within the chemically modified surface layer, could affect the FE features of the $PbTiO_3$ samples, which were detected by the *I–E* hysteresis loop and the pyroelectric current measurements.

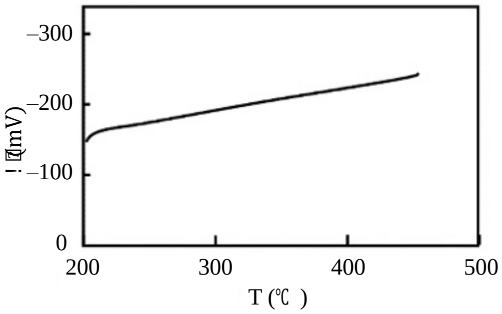

Figure 8. The electromotive force ϵ vs. temperature. The sample was oxidized at T = 650 °C and cleaved to produce the asymmetric configuration of the oxidized sample: electrode–surface layer–$PbTiO_3$ bulk–electrode. The sequence and composition of chemically variant sub-layers are described in the text.

We obtained similar measurements of the local electromotive force on the nanoscale using AFM potentiometry for the oxidized crystal, which was cleaved in situ (for a schematic of the measurement see Figure 9a). The distribution of the potential in the surface region (Figure 9b) allows, without the information from an SIMS depth profile, calculation of the strength of the local electric field (see Figure 9c). The value is higher than the coercive field for $PbTiO_3$. Therefore, we can make the assumption that in this region the polarization of $PbTiO_3$ should be permanently oriented in the direction of the built-in fields.

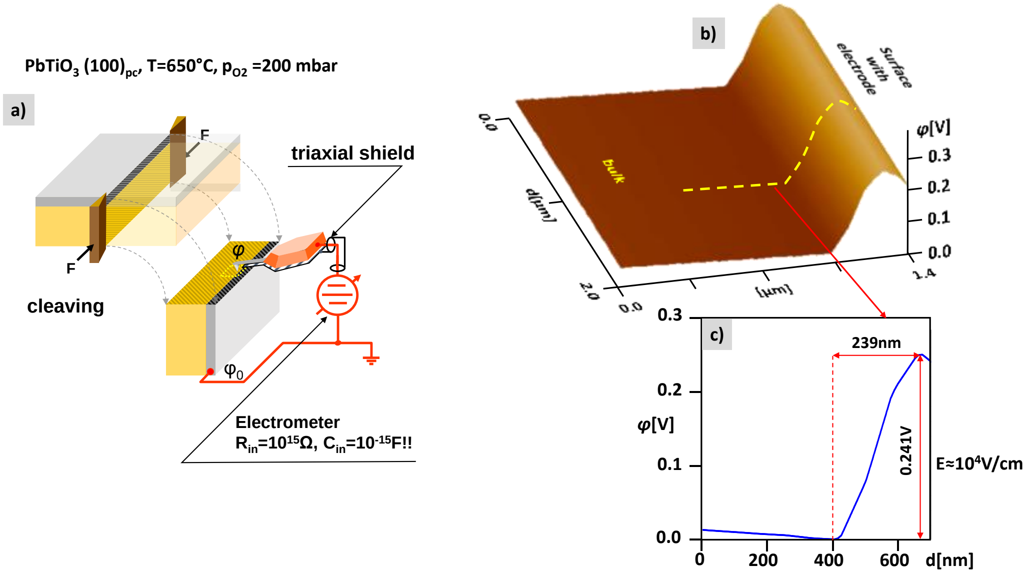

Figure 9. (**a**) Schematic illustration of the electrometric determination of the electromotive force in the surface region of a cleaved $PbTiO_3$ crystal (the sample was oxidized at T = 650 °C). The mapping of the potential distribution in the surface region close to the electrode is presented in (**b**). The potential drop in this region (**c**) allows the calculation of the local electric field, the strength of which reaches a value higher than the coercive field.

3.4. Surface Layer, XPS Studies

Before we explain the models that allow a better understanding of the origin of the pinning of the spontaneous polarization in a lead titanate crystal, we analyze the differences in the electronic structure, chemical composition, crystallographic and defect structure between the surface of the crystal as grown (that does not exhibit self-poling effects) and the upper part of these crystals after thermal treatment (where self-poling occurs). A prerequisite is the proof that the used crystals possess excellent quality, primarily because they concern crystals grown by spontaneous crystallization from flux. Although the X-ray diffraction pattern of our crystals shows the typical lattice parameter [40] and the dielectric and Raman measurements a correct sequence of the phase transitions [41,42,58], from the chemical point of view, the composition of the crystal due to the method flux growth shows a surplus of Pb. Most scientific articles dedicated to FE properties or defect chemistry are based on such prepared crystals [44,59–63], although some refinements are available [64]. Using the chemical analysis ICP-OES (for determination of the concentration Ti and Pb) and infrared spectroscopy (for the analysis of the amount of oxygen), it was found that the chemical formula of our crystal can be written as follows: $Pb_{1.02\pm0.02}Ti_{0.96\pm0.012}O_{3\pm0.04}$. This additional incorporation of a few percent of Pb in the matrix of the crystal can be explained in two ways: either additional PbO will create a stacking fault in the matrix, $(PbO)_{0.06}PbTiO_3$ [65–68], where an equidistant distribution of PbO planes will generate an RP phase [40]; or, if the valence of Pb is reduced to 4+, an anti-structural disorder can be observed in the matrix [41,42]. Due to the similar ionic radii of Ti^{4+} and Pb^{4+}, the lead cations can occupy the position of titanium, and the correct formula, in this case, could be $Pb^{2+}Ti_{0.96}Pb^{4+}{}_{0.04}O_3$ [41,43]. In fact, the stoichiometry analysis of XPS spectra of in situ cleaved $PbTiO_3$ crystals shows that the surface layer is enriched by 25% in Pb (compare Figure 10). This discrepancy in fifty/fifty termination between PbO and TiO_2 can only take place if the cleaving plane runs along a stacking fault [67,68].

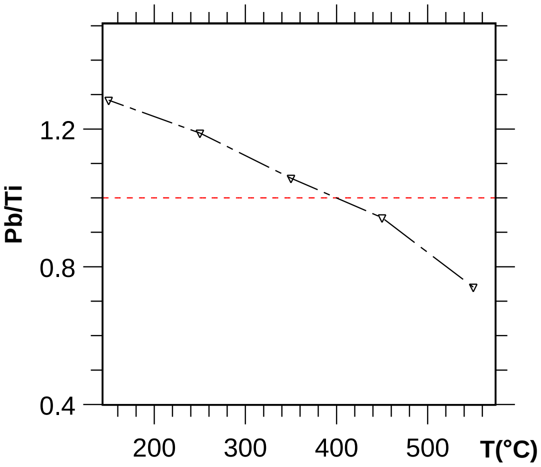

Figure 10. The change in the relative stoichiometry of the cations on the surface layer induced by the thermal treatment (under UHV) of the cleaved $PbTiO_3$ single crystal as determined by in-operando XPS measurements.

Our XPS analysis shows the typical shapes of the core lines of $PbTiO_3$. The O1s line is a singlet, and the shapes of Ti2p and Pb4f are single doublets whose energetical position can be assigned to cations with valence 2+ for Pb and 4+ for Ti (Figure 11; however, no evidence for the presence of Pb^{4+} was found. The absence of an occupied state in the valence band (VB) and the correct width of the band gap (BG, here > 3 eV, see lower right panel of Figure 11) allow for the classification of the surface layer as a dielectric. It should be noted that, for the cleaved surface with a conchoidal morphology of the cleavage/fracture, no additional compounds of the O1s line (typical for physical and chemical adsorption) were found, and the absence of the C1s peak indicates that the surface is free from carbon contamination. Such a reference surface was annealed in situ under the UHV conditions and oxidized ex-situ. Using thermogravimetric analysis (TGA), we have determined that the maximal annealing temperature in oxidizing conditions should not be higher than 600–650 °C, otherwise evaporation of PbO from $PbTiO_3$ would occur.

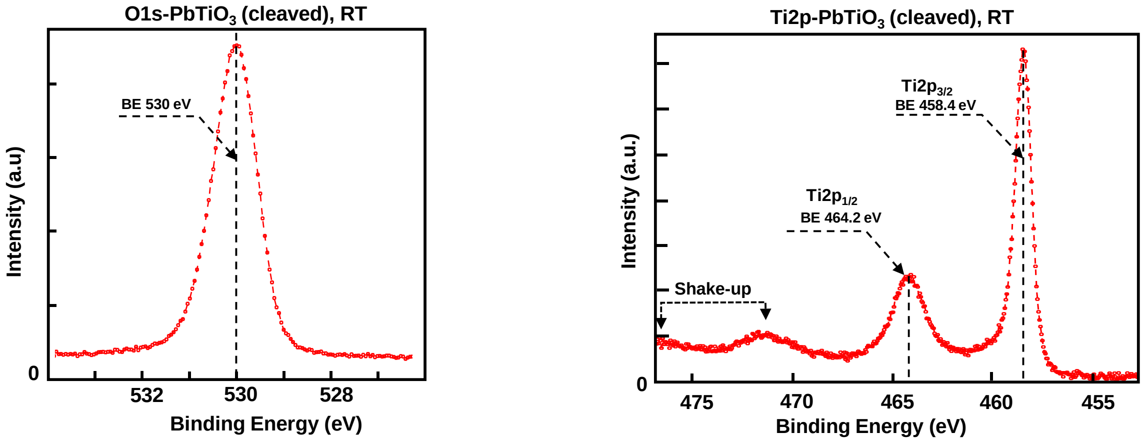

Figure 11. *Cont.*

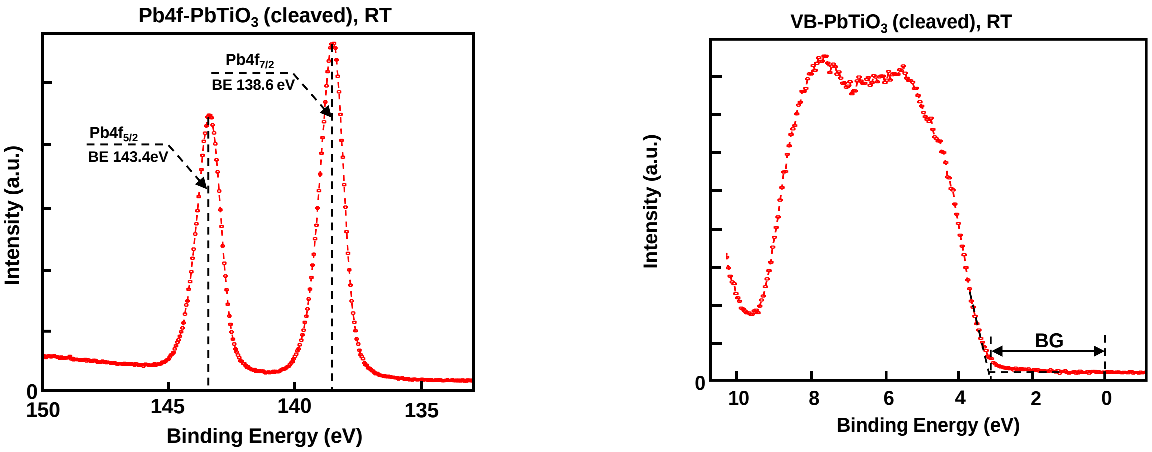

Figure 11. XPS$_{\text{Al k}\alpha}$ spectra of core lines (O1s, Ti2p, Pb4f) and VB region of an in situ cleaved PbTiO$_3$ crystal.

We have studied the changes induced by thermal treatment of the surface or in the surface region by XPS, EDX/TEM, and AFM. The ex-situ oxidation leads to a dramatic increase in contaminants that can be identified by additional compounds appearing in the O1s and C1s lines. Only the Pb 4f core line, after annealing in an oxygen-rich environment, shows an essential change in its shape (Figure 12). The precise difference analysis, relative to the reference Pb4f line of the cleaved (clean) crystal, shows the existence of two peaks with higher and lower binding energy. A search in the literature [41,42] suggests that additional oxide (PbO) and metallic lead have been created in the surface layer of oxidized crystal.

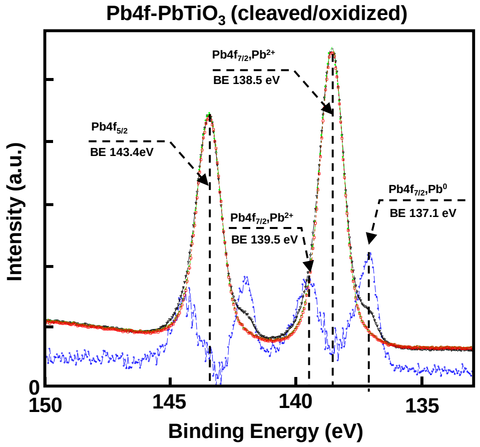

Figure 12. Difference between the reference spectra of the Pb4f core line of the cleaved sample (red and green) and the oxidized crystal (dark). The spectra were normalized. The difference spectrum (blue) was magnified by a factor of 4.

In fact, after a long time of contact between PbTiO$_3$ and oxygen at high temperatures, we found (using EDX), in the materials removed from the surface layer/regions via mechanical polishing, that a specific population of micro-crystallites does not possess any Ti ions and that their chemical formula may be typical for PbO or Pb (Figure 13). We have presented a similar conclusion about the surplus of Pb in the upper part of the surface layer by the analysis of the SIMS depth profile [57]. Moreover, we have found an anti-correlation between the geometrical position of the surplus of lead and enrichment with Ti (which can be observed in the deeper region of the surface layer between 20–45 nm). Due to the small non-stoichiometric limit for cations in the matrix of PbTiO$_3$, these materials cannot maintain the perovskite structure and must recrystallize or remain amorphous. The creation of the crystallites on a cleaved surface with a distinct morphology (which can be observed with

AFM [57]) and the change of X-ray diffraction pattern (see our previous operando investigation of the crystallographic structure [40]) does not leave any doubt that the surface region is subject to recrystallization from $PbTiO_3$ into R–P and TiO phases. These observations about the complicated chemical and crystallographic changes in the surface layer/regions should be considered when analyzing the self-poling's origin in oxidized $PbTiO_3$ crystals. Although our data confirm that a chemical transformation occurs in the surface layer, and we have information about the stacking sequence (chemistry) in the upper and deeper layers, we do not know which type of ions (cations/anions) can migrate out-of-plane for those moderate temperatures and generate this solid-state reaction.

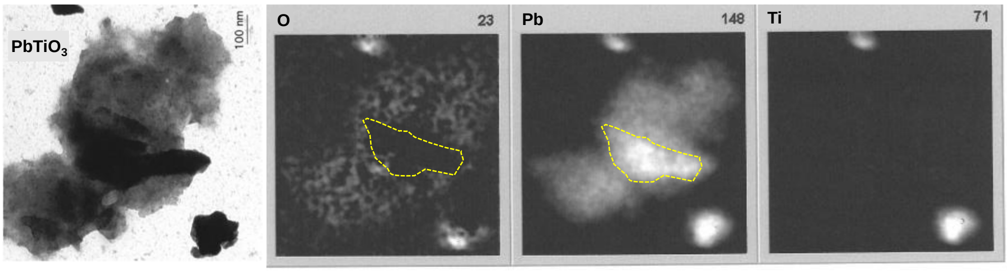

Figure 13. TEM photograph (left) and EDX mapping of microcrystals removed from the surface of oxidized $PbTiO_3$ crystal by mechanical polishing. The dashed line marks the area with low oxygen and high lead concentrations.

The XPS investigation in situ on cleaved crystals showed that at 200 °C segregation of Pb can be observed (Figure 10). Because such migration of Pb in the perfect perovskite matrix is high unlikely for temperatures lower than 500 °C, it is probable that the extremely high density of extended defects in $PbTiO_3$ crystals [59,67,68], with specific crystallographic and electronic properties, may play an important role in the easy diffusion of Pb cations (see, e.g., ref. [69]).

3.5. DFT Calculations

To quantify the effect of an asymmetric environment on a Ti atom in an octahedral cage of oxygen atoms, we performed DFT calculations using a generalized gradient approximation [47] that can offer a reliable description of $PbTiO_3$ structural properties. Employing the full-potential LAPW method [48] in the thin-film setup [70], we studied a TiO_2-terminated nine-layer $PbTiO_3$ film with the optimized lattice parameters of the FE structure but set the polarization to zero. Thus, in each plane, the oxygen and metal atoms are at the same vertical position.

Thereafter, we monitored the total energy of the system as a function of the vertical displacement of the central Ti atom. Due to the strong depolarization field in the structure, the Ti prefers to stay in the plane center (blue curve in Figure 14). To introduce an asymmetry in the system, we then replaced one of the surface TiO_2 layers by PbO (right panel of Figure 14). Allowing the central Ti atom to relax again, we found that it became shifted by 0.03 Å away from the PbO terminated side, resulting in a gain of about 6 meV per in-plane unit cell (red curve in Figure 14). Further relaxation of the whole film resulted in a configuration with a finite, non-switchable dipole moment, corresponding to a polarization of $0.007\ \mathrm{C\ m^{-2}}$. This value is compatible with a 0.03 Å shift of the Ti^{4+} ions in the TiO_2 layer but is significantly lower than the polarization of bulk $PbTiO_3$, indicating that, in the actual surface region, more extended defects (e.g., additional TiO_2-rich phases or Pb^0) must be present.

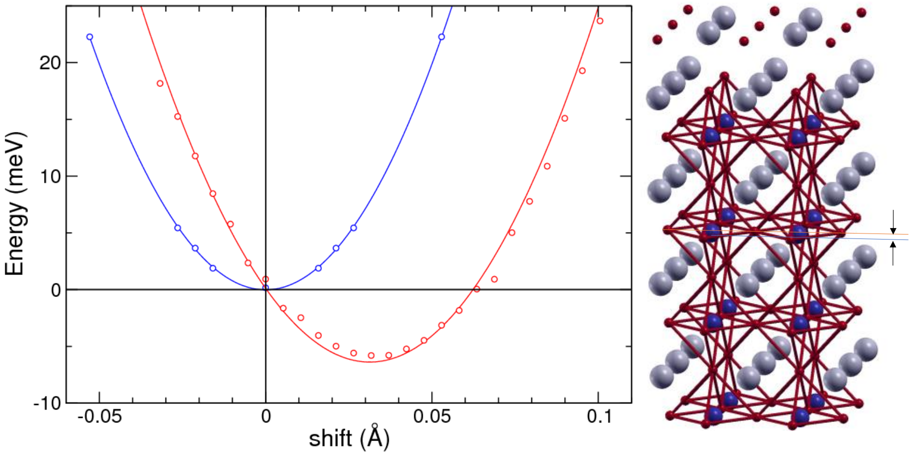

Figure 14. Variation of the total energy as a function of the shift of the central Ti atom for a TiO_2-terminated nine-layer $PbTiO_3$ film (blue) and a film with one of the surface layers replaced by PbO (red) obtained from DFT calculations. The PbO-terminated film structure is shown in the right panel: grey/blue/red spheres indicate Pb/Ti/O atom positions, respectively, and arrows mark the shifted planes.

3.6. Model Calculations

Following the methodology outlined in Section 2.5 we derive here the boundary conditions for the normal component of the vector D on the ferroelectric–self-polarized layer interface. It can be seen from Figure 2d that field and polarization vectors are directed along the z axis, i.e., D = $D\mathrm{i}_z$, E = $E\mathrm{i}_z$, P = $P\mathrm{i}_z$. In this case, the boundary conditions for the continuity of the normal component of vector D on the FE–self-polarized layer interface read as follows:

$$D_b = D_f, \tag{1}$$

where D_b and D_f are, respectively, the z-components of electric displacement vectors in the self-polarized (we may call it the blocking layer, hence index b) and FE layers. These are given by the following material equations:

$$D_b = \varepsilon_0 \varepsilon_b E_b,\ D_f = \varepsilon_0 E_f + P, \tag{2}$$

where E_b, E_f and $P = P_f + P_b$ are, respectively, the average electric fields in the blocking (self-polarized) and FE layer and the average polarization of the FE layer, consisting of switchable P_f and non-switchable P_b polarizations. Here, ε_0 is the vacuum permittivity in SI units. We note that the seemingly asymmetric nature of the material Equation (2) actually comes from the additional boundary conditions [49,53]. The equation for D_b contains only the blocking layer polarization $P_b = \chi_b E_b$ (here $\chi_b = \varepsilon_0\ (\varepsilon_b - 1)$ is the dielectric susceptibility of the blocking layer), while that for D_f includes both components, P_b and P_f. This shows that, while the ferroelectric layer dipoles can be spontaneously and coherently oriented (thus forming a spontaneous polarization), those of the non-ferroelectric (blocking in our case) layer cannot. On the other hand, the constant polarization P_b of the blocking layer acts as a form of external electric field, which penetrates into the ferroelectric layer as well. At the same time, it can be shown that the spontaneous polarization does not exist beyond the actual ferroelectric layer.

Equation (2), along with (1), determines the polarization coupling in the blocking and ferroelectric layer, i.e., they describe the mutual influence of the above two layers. To make this more evident, we rewrite expression (1) with respect to (2) explicitly as $E_b = (\varepsilon_0 E_f + P_f + P_b)/(\varepsilon_0 \varepsilon_b)$. Thus, system (2) should be augmented by the equation for the electric potential across the structure in Figure 2e [51]

$$dE_b + hE_f = (d + h)E, \tag{3}$$

where E is the external applied field, and d and h are the thicknesses of blocking and FE layers, respectively. Equation (3) permits to express E_f as a function of E and E_b

$$E_f = -\frac{d}{h}\,E_b + \left(1 + \frac{d}{b}\right)E. \tag{4}$$

Combining Equation (2) with respect to (1) and (4), we obtain the set of equations for the description of the hysteresis loop $P(E)$ of the whole structure, having at our disposal the "internal" (i.e., that in the FE layer) $P(E_f)$. These equations read for $d/h << 1$

$$E = E_f + \frac{d}{h}\frac{P}{\varepsilon_0\,\varepsilon_b},\; P = P_f + P_b. \tag{5}$$

The "internal loop" $P(E_f)$ can be chosen in the arbitrary form. This form should, however, reflect the property in which an electric field is swept between large positive and negative values. The polarization must approach the spontaneous polarization $\pm Ps$, which is realized when all FE dipoles are completely aligned by the external field. We note here that the value of P_S for our structure would be affected by the non-switchable polarization P_b.

The latter property of the hysteresis loop is obviously present in the Landau expansion $aP + bP^3 + E_f = 0$. However, the problem with this expansion is that, near to the coercive field E_c, the derivative dP/dE goes to infinity, which is unphysical. The reason for this is that, in our experiment, we measure the current loops, i.e., the dependence of current density $j = dP/dt$ on the electric field E. Because we sweep the external electric field linearly with time $E = at$ to measure the hysteresis loop, the derivative dP/dt becomes $dP/dt = a\,dP/dE$, i.e., it is proportional to the field derivative dP/dE of polarization. This means that realistic dependence $P(E_f)$ should have finite derivatives dP/dE_f everywhere.

Such a realistic hysteresis loop can be taken as an empirical dependence [71]. We have

$$\begin{gathered} P^{+}(E) = P_S \tanh\frac{E-E_c}{2\delta} + f(E), \\ P^{-}(E) = P_S \tanh\frac{E+E_c}{2\delta} + f(E),\;\; P^{+}(E) = -P^{-}(-E) \end{gathered} \tag{6}$$

where $f(E)$ is an arbitrary odd function, which is to be chosen from the best fit to experiment. Here δ is the fitting parameter and E_c is the coercive field. The plots of the functions $P^{\pm}(E)$ (6) and their derivatives $dP^{\pm}/dE$ are reported in Figure 15 for $f(E) = 0$ (panels (a) and (c)) and for $f(E) = aE$ (panels (b) and (d)). It is seen that hysteresis loops and their derivatives resemble those measured in the experiment. Additionally, the derivatives dP/dE have the same magnitude.

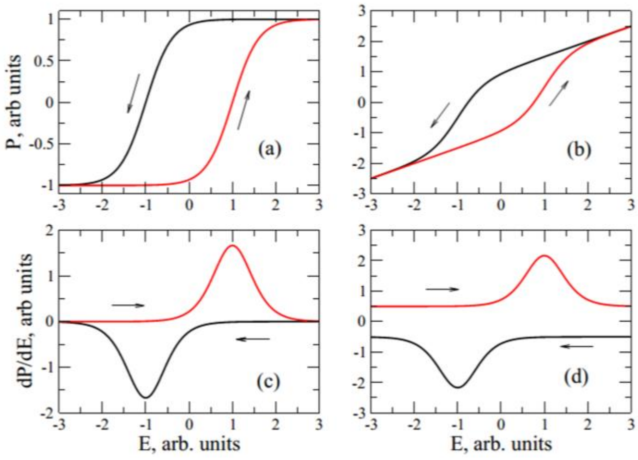

Figure 15. The hysteresis loops $P^{\pm}(E)$ (6) and their derivatives $dP^{\pm}/dE$ for $P_S = 1$, $\delta = 0.3$, $E_c = 1$. Panels (**a**,**c**) correspond to $f(E) = 0$, panels (**b**,**d**) to $f(E) = 0.5E$. Arrows show the external field sweep directions.

Now we are in a position to calculate the real observable hysteresis loops corresponding to Figure 2d (symmetric situation) and Figure 2e (asymmetric situation). To do so, we observe that spontaneous polarization P_S is affected by the built-in P_b, i.e., we should substitute in Equation (6) $P_S \to P_S + P_b$ in $P^+(E)$ and $P_S \to P_S - P_b$ in $P^-(E)$. We note here that, for the symmetric structure depicted in Figure 2d, the term P_b is cancelled as we have $P_S + P_b - P_b = P_S$ for both branches $P^{\pm}(E)$ of the hysteretic curve so that it will be symmetric, like that shown in Figure 15. Substitution of the thus-modified loops (6) into Equation (5) generates the desirable "external" loops $P(E)$. These are plotted in Figure 16.

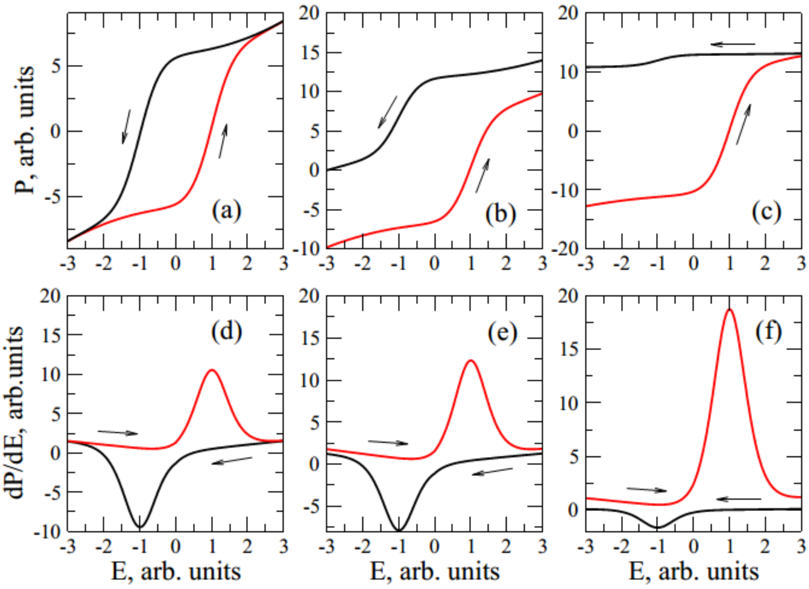

Figure 16. The real hysteresis loops $P(E)$ (5) and their derivatives dP/dE for $P_S = 6.0$, δ = 0.3, $E_c = 1$, $d/(h\ \varepsilon_b) = 0.01$, $f(E) = 0.02E^3$. Panels (**a**,**d**) correspond to $P_b = 0$ (complete compensation or absence of blocking layer), panels (**b**,**e**) to $P_b = 1 << P_S$ (incomplete compensation), and panels (**c**,**f**) correspond to experimental uncompensated case $P_b = 5 \approx P_S$. Arrows show the external field sweep directions.

Similar to Figure 15, we plot both $P(E)$ curves and their derivatives dP/dE, proportional to the current density. The case $P_b = 0$ is reported in panels (a) and (d) of Figure 16. This situation corresponds either to complete compensation (panel (d) of Figure 2) or to the absence of blocking layer. This case, similar to Figure 15, corresponds to the symmetric hysteresis loop and the same amplitudes of the currents in panel (d) of Figure 16. In this case, for $E \to \pm\infty$, the corresponding asymptotic values of $P^+(E)$ and $P^-(E)$ are the same. Panels (b) and (e) of Figure 16 report the situation of the incomplete compensation of P_b, when either P_b in a single layer (panel (e) of Figure 2) is smaller than the saturation (spontaneous) polarization of the FE layer P_S or in the situation in which we do not completely cut one of the blocking layers in our structure. Here we note that, at $E \to \infty$, the branches $P^+(E)$ and $P^-(E)$ merge, similarly to the case of $P_b = 0$ (Figure 15), while at $E \to -\infty$ $P^+(E) \neq P^-(E)$, with their difference being related to the presence of P_b. If we change the sign of P_b, our picture will be opposite: at $E \to -\infty$ $P^+(E) = P^-(E)$, while at $E \to \infty$ we find $P^+(E) \neq P^-(E)$. The current, proportional to derivative dP/dE is now slightly larger for the left-to-right direction of the field sweep, while in the opposite direction it is smaller.

Finally, the panels (c) and (f) of Figure 16 display the experimental situation, related to the panel (e) of Figure 2, i.e., to the fully uncompensated P_b. We choose $P_b = 5$ to be slightly smaller than $P_S = 6$. In coincidence with the experimental situation, on panel (f) of Figure 16 we can see a large asymmetry in the current magnitudes in back-and-forth directions of the field sweep. This asymmetry is related to the presence of an uncompensated (i.e., "tail-to-tail" or "head-to-head" oriented) built-in polarization relative to the spontaneous polarization. Panel (c) shows the physics of the process. Namely, for $P_b > 0$ (as we choose here), it is directed in the positive direction of z axis, being parallel to the external field,

E, as shown in Figure 2. Thus, when we sweep the field in Figure 16c from left to right (which corresponds to the positive direction of z axis, as in Figure 15), the oppositely directed polarization in the FE layer adjusts to the field direction so that all polarization in the FE layer has a similar direction to P_b, creating a stable (in this case "head-to-tail") configuration. This situation is reflected by the red curve in Figure 16c. When we sweep the field back, the built-in polarization P_b stays intact, while the FE polarization tends to align with the (opposite to P_b) field direction, thus creating an energetically unfavorable "tail-to-tail" configuration. This is why, for this sweep direction, the system resists the creation of an energetically unfavorable configuration, i.e., it has a very large coercivity so that the polarization does not change much even for large negative fields. This generates a very weak variation of the polarization in this branch which gives a much smaller (than that of the red curve in the Figure 16c, corresponding to the direct sweep of the external electric field) derivative dP/dE. This, in fact, demonstrates the role of the uncompensated built-in polarization.

4. Discussion

The assumption that the surface layer consists of several components allows for the interpretation of the built-in polarization properties in the $PbTiO_3$ crystal under investigation. The presence of a built-in polarization is manifested by the asymmetric shape of the *I*–*E* hysteresis loop and the pyroelectric current peak.

The standard, as-grown $PbTiO_3$ samples show a symmetric *I*–*E* hysteresis loop, a lack of pyrocurrent, no electromotive force, and a spontaneously formed ferroelectric domain pattern structure.

The suppressed FE properties were detected in the thermally treated "symmetric" samples. In this case the modified surface layer envelopes the crystal bulk. The thicknesses of the surface region with PbO and TiO_2 enrichment can be determined from the SIMS profile analysis shown in our previous paper [57]. Using this value and the knowledge of the macroscopic electromotive force, we can calculate gradients of the electromotive force in the surface layer and thus determine the strength of the local electric field—$d\epsilon/dL \approx 10^5$ V cm^{-1}. Therefore, the E_{SL}, which is essentially stronger than the FE coercive field E_C, induces the polarization P_{SL} within the surface $PbTiO_3$ sublayer. Hence, the P_{SL} is directed outward and fixed by the surface layer field E_{SL}. The FE polarization of the bulk is screened by the latter surface layer features, despite the fact that the bulk FE domains preserve their ability to reorient. Moreover, we deduce that the surface layer field E_{SL} appears in the sample below both electrodes. This means that these effects are responsible for the relatively low value of $P_S \cong 0.05$ C m^{-2} (see Figures 6b and 7b). As a result of this, the true FE properties of the thermally treated $PbTiO_3$ samples are hidden below the oxidized surface layer, which has been generated by the thermal treatment. This, in turn, results not only in a change in the distribution of Pb and Ti ions but also in a change in the concentration of Pb^{2+} ions and metallic Pb^0 in the surface layer (out-of-plane).

The "asymmetric" samples were produced by cleaving. One electrode was then placed on the multi-component surface layer of a sample and the other electrode was deposited directly on the FE bulk (Figures 1c and 2c). For such an "asymmetric" configuration one can obtain the direct access to the bulk as well as to the surface layer. The sample response to the triangular voltage sweep was determined by two contributions: (1) the FE polarization P_{FE} =P_f (see Section 3.6 devoted to our model calculations) related to the reorientable FE domains in the bulk and (2) the fixed, i.e., non-reorientable P_{SL}=P_b (see also Section 3.6). When the external field is parallel to the resultant $P_{FE} > 0$, then the measured electric current signal is low as there is a negligible change in the density of the bound electric charge. When the external field is anti-parallel to the resultant $P_{FE} > 0$, then the measured electric current signal is high due to the substantial change in the above charge density. Hence, two different values of P_S were actually determined for the "asymmetric" case, i.e., $P_{S,2}$ equal to 0.015 C m^{-2} and $P_{S,1}$ = 0.56 C m^{-2}. The first value is related to the polarization screened by the field in the surface layer. The second is related to the FE domains in the bulk.

We would like to point out that similar oxidation and reduction procedures were performed for $PbZrO_3$ crystals, where the Pb and O vacancies amounts had been deliberately varied by thermal treatment [72–74]. It has been shown that the FE polarization, determined from the pyroelectric effect and the D–E hysteresis loop, was affected by the subsystem of these defects. However, the temperature range of the FE phase occurrence did not change.

We propose to describe the polarization features of the $PbTiO_3$ samples with respect to the electromotive force's temperature dependence $\epsilon(T)$ = A + BT using the Nernst equation. The Nernst equation is applied to fuel and galvanic or concentration cells, mainly in the case of gaseous species transported in them. However, one can find reports where the migration of metal ions is analyzed [75–77]. Hence, we presume that the occurrence of the electromotive force for the $PbTiO_3$ crystals can be explained by the Nernst equation, as the concentration of Pb ions was different for the near-electrode regions of the "asymmetric" (i.e., electrode | $Pb\cdot(PbO\cdot(PbTiO_3)_n)$ | $PbTiO_3$ | TiO_2 | $PbTiO_3$ | electrode) samples. The electromotive force ϵ of a cell can be qualitatively expressed as

$$\epsilon = \epsilon_0 - \frac{RT}{3F} ln \frac{a_{Pb^0}}{a_{Pb^{2+}TiO_3}} \tag{7}$$

where R, T, and F denote the gas constant, the absolute temperature, and the Faraday constant, respectively. The a_{Pb^0} and $a_{Pb^{2+}TiO_3}$ denote the Pb^0 (i.e., in the near-electrode regions of a sample) and $PbTiO_3$ (sample bulk) activities, respectively. Any quantitative estimation of the electromotive force ϵ would require a separate series of experiments.

The earlier XRD study [41] has shown that the surface layer crystal lattice structure was different from the standard perovskite ABO_3 structure. The oxidized samples consist of a mixture of $PbTiO_3$ and the $PbO\cdot(PbTiO_3)_n$ phases with n = 1, 2, …, 6, and TiO_2-rich phases [40,57]. Hence it may be concluded that the surface layer transformation, occurring via solid-state phase reaction, results in a successive increase in the number of PbO planes and, at high temperatures, to the reduction of surplus PbO to metallic lead. Such a restructuring of the crystal lattice related to the Pb^0/Pb^{2+} ratio redistribution can lead to the formation of the concentration cell. One can deduce that the electromotive force ϵ~0.3–0.6 V is of electrochemical origin. Because ϵ appears in a thin surface, an essential electric field E_{SL}~10^5 V cm^{-1} can be found. We postulate that E_{SL} is sufficiently high to induce a fixed (i.e., non-reorientable) electric polarization within the intermediate $PbTiO_3$ sublayer, which may be identified as lying 20–25 nm below the outer surface of the oxidized sample (see SIMS profile of the oxidized $PbTiO_3$ crystal [57] and compare Figure 9).

The case of spontaneous non-zero net polarization has been discussed in the literature. We would like to note that V. M. Fridkin reported the effect of "natural" polarization for FE materials, e.g., for ferroelectric SbSI crystals [45]. The features of the internal field distribution, which influence the net polarization, can be determined by two mechanisms. One is related to the participation of the surface levels in screening. The second is related to the charge of the surface levels and causes a curvature of the energy bands [29,45]. This curvature appears at the ends of the crystal and can induce a unipolarity of ferroelectric crystals. The occurrence of the net $P_S \neq 0$ is reversible and depends on temperature, i.e., the net P_S disappears after heating the samples above the FE–PE phase transition temperature. The net P_S forms in such a way that it can also be varied by applying an external electric field to the sample. Such FE samples exhibit standard D–E hysteresis loops as well as pyroelectric currents.

However, the case studied in this work is qualitatively different. The samples used in our experiment were prepared in two steps. In the first step, they were thermally treated and, as a result, a chemically modified surface layer was obtained. The fabricated samples were spatially symmetric. In the second step they were adapted by mechanical intervention, i.e., one side of the sample was removed. Consequently, an asymmetric, permanent, and chemically inhomogeneous structure of the lead titanate sample was obtained.

The chemical effects related to the ions' migration, determined the measured effective polarization of the $PbTiO_3$ crystals. The microscopic insight into the surface layer composition supports the former XRD study [40] and the XPS spectroscopic measurements. The $PbTiO_3$ crystal, heated for several hours under oxidizing conditions, showed that PbO-rich Ruddlesden–Popper phases as well as TiO_2-based Magnelli phases are formed in the vicinity of the surface of the samples. In addition, the formation in the surface layer of metallic Pb can be determined using XPS analysis. Hence, the occurrence of the layered structure electrode | surface layer | $PbTiO_3$-bulk | electrode seems to be justified. These products are consistent with the result of the SIMS test [57] carried out for $PbTiO_3$, where the termination with the PbO–Pb planes of the crystal can be derived from the XPS analysis. It is noteworthy that our experiment was conducted at a moderate temperature in order to induce ionic migration towards the surface of the crystal as well as to obtain a structurally modified surface layer. We conclude that the strong electric field E_{SL}, caused by the variation in the Pb^0/Pb^{2+} metal/ions ratio, induced a strong electric field, which fixed the polarization P_{SL} within the $PbTiO_3$ sublayer. Simultaneously, the inner part of the bulk remained unaffected, with the FE order unchanged.

The surface layers, electrodes and interfaces play an important role in the FE properties of the ABO_3 perovskite materials at the micro- and nanoscale [78]. It was found that the FE order stability can persist down to structures with very thin layers (as thin as several nanometers), which corresponds to about 5–10 atomic layers of the perovskite structure [8,10,15,16,75,79]. The structures were influenced not only by the interface appearance but also by the surface chemical composition and the related structural defects such as the oxygen vacancies in it. Note that the influence of the ensemble of defects and impurities on the electronic structure and polarization has been studied experimentally [7,9,26,27,80] and theoretically by ab initio calculations [6,8,81–84]. The value of the built-in polarization in the surface layer is influenced to a great extent by the type of electrodes, e.g., metallic Pt and oxide-type $SrRuO_3$. Moreover, the type of termination planes, i.e., PbO and TiO_2, affects the dipole moments within the crystal surface layer. Their interaction with the FE polarization in the bulk determines the stability of the surface layer polarization. It has been shown that the surface layer polarization has a tendency to align inward or outward of the surface plane [10,79,85,86].

From this point of view, the occurrence of polarization in the ABO_3 sublayer, thinner than 10 nm, is fully justified. The presence of such an ordered sublayer has been inferred from the SIMS, XRD, and electrical tests on the thermally treated $PbTiO_3$ samples. The necessary internal electric field that induces this polarization direction has been determined by the formation of PbO and TiO_2 planes as a result of ion migration which, in turn, has been initiated by thermal treatment. Moreover, the obtained results suggest that the fabricated samples show an arrangement which corresponds to a homo-epitaxial structure, i.e., a $PbTiO_3$ thin layer covered with PbO planes and interfaced from the $PbTiO_3$ bulk by TiO_2 planes.

Hence, this contribution to the electric polarization is dominated by the internal electric field. Therefore, we call this phenomenon the "self-polarization" effect. This self-polarization is manifested within the thin sublayer of the perovskite structure. It is induced and sustained by the internal field, originating from the chemically inhomogeneous surface layer, which envelopes or wraps the structurally proper perovskite bulk of the $PbTiO_3$ crystal. Such a layer appears when the sample is cooled through the PE–FE transition, after high-temperature oxidation. The polarization appears due to the interaction of charged interfaces between the Pb-rich and Ti-rich planes [3,10,29,30,40]. In accordance with DFT ab initio calculations and the asymmetry of the lattice structure, the PbO-terminated surface provides a shift of the relaxed Ti ions with respect to the oxygen octahedra. Hence, this shift corresponds to the occurrence of electric polarization within the surface layer. In the case of the "symmetric" sample configuration, these fields and surface layer polarization compensate each other when the macroscopic, electrical measurements are conducted. Only after removing the surface layer part, are unbalanced contributions from the surface layer on one side and from the unwrapped bulk on the other side obtained. Such an asymmetric structure is manifested by the electromotive force and by the asymmetric *I*–*E* hysteresis loop. Hence, we suggest that it is possible to produce a non-zero net polarization in $PbTiO_3$ crystals without the preliminary application of an external electric field [29,30,32].

5. Conclusions

In summary, using both experimental and theoretical arguments, we have shown that both structural and chemical modification of the $PbTiO_3$ surface layers can lead to self-polarization. In our studies, we have observed that thermal treatment under oxidizing conditions induces the migration of Pb ions and PbO complexes towards the near-surface regions. Moreover, we have also noticed that new Pb-rich structures, for example, PbO planes and/or Ruddlesden–Popper phases appear to exhibit anti-correlations with the Ti-rich regions within the surface layer. We have also found that the induced gradient in Pb and Ti atomic concentrations in the surface layer leads to a built-in electric field $E_{SL} \approx 10^5$ V/cm, which is stronger than the coercive field E_C related to the FE bulk of $PbTiO_3$.

Moreover, we maintain that the "self-polarization" effect appears due to the interaction between the Pb-rich and Ti-rich layers, when the sample is cooled through the PE–FE transition, after oxidation at high temperature.

We postulate that it is feasible to produce a non-zero net polarization in $PbTiO_3$ crystals without the preliminary application of an external electric field. This is possible due to the unbalanced contribution both from the chemically modified surface layer and the unwrapped FE bulk.

Author Contributions: Conceptualization, investigation, writing—original draft preparation, K.S.; visualization and formal analysis, C.R. and K.S.; validation and writing—review and editing, C.R., K.S. and G.B.; DFT calculations, G.B.; XPS analysis, J.S., M.P. and A.M.; thermodynamic calculation, discussion, V.A.S. All authors have read and agreed to the published version of the manuscript.

Funding: This work was partially supported by the German Research Foundation (DFG) in framework of the project SFB917.

Data Availability Statement: Data are contained within the article.

Acknowledgments: The authors are thankful to K. Wójcik for the delivery of $PbTiO_3$ crystals.

Conflicts of Interest: The authors declare no conflict of interest.

References

1. Waser, R.; Boettger, U.; Tiedke, S. (Eds.) *Polar Oxides*; Wiley-VCH Verlag GmbH & Co, KgaA: Weinheim, Germany, 2005.
2. Waser, R.; Dittmann, R.; Staikov, G.; Szot, K. Redox-Based Resistive Switching Memories–Nanoionic Mechanisms, Prospects, and Challenges. *Adv. Mater.* **2009**, *21*, 2632–2663. [CrossRef]
3. Pentcheva, R.; Pickett, W.E. Electronic phenomena at complex oxide interfaces: Insights from first principles. *J. Phys. Condens. Matter* **2010**, *22*, 043001. [CrossRef] [PubMed]
4. Chirila, C.F.; Stancu, V.; Boni, G.A.; Pasuk, I.; Trupina, L.; Filip, L.D.; Radu, C.; Pintilie, I.; Pintilie, L. Controlling polarization direction in epitaxial $Pb(Zr_{0.2}Ti_{0.8})O_3$ films through Nb (n-type) and Fe (p-type) doping. *Sci. Rep.* **2022**, *12*, 755. [CrossRef] [PubMed]
5. Mtebwa, M.; Setter, N. Control of Self-Polarization in Doped Single Crystalline $Pb(Zr_{0.5}Ti_{0.5})O_3$ Thin Films. *Integr. Ferroelectr.* **2022**, *230*, 148–155. [CrossRef]
6. Meyer, R.; Liedtke, R.; Waser, R. Oxygen vacancy migration and time-dependent leakage current behavior of $Ba_{0.3}Sr_{0.7}TiO_3$ thin films. *Appl. Phys. Lett.* **2005**, *86*, 112904. [CrossRef]
7. Szot, K.; Speier, W.; Bihlmayer, G.; Waser, R. Switching the electrical resistance of individual dislocations in single crystalline $SrTiO_3$. *Nat. Mater.* **2006**, *5*, 312–320. [CrossRef]
8. Duan, C.-G.; Sabirianov, R.F.; Mei, W.-N.; Jaswal, S.S.; Tsymbal, E.Y. Interface Effect on Ferroelectricity at the Nanoscale. *Nano Lett.* **2006**, *6*, 483–487. [CrossRef]
9. Tybell, T.; Ahn, C.; Triscone, J.-M. Ferroelectricity in thin perovskite films. *Appl. Phys. Lett.* **1999**, *75*, 856–858. [CrossRef]
10. Meyer, B.; Vanderbilt, D. Ab initio study of $BaTiO_3$ and $PbTiO_3$ surfaces in external electric fields. *Phys. Rev. B* **2001**, *63*, 205426. [CrossRef]
11. Watanabe, Y. Theoretical stability of the polarization in a thin semiconducting ferroelectric. *Phys. Rev. B* **1998**, *57*, 789–804. [CrossRef]

12. Junquera, J.; Ghosez, P. Critical thickness for ferroelectricity in perovskite ultrathin films. *Nature* **2003**, *422*, 506–509. [CrossRef]
13. Kim, D.J.; Jo, J.Y.; Kim, Y.S.; Chang, Y.J.; Lee, J.S.; Yoon, J.-G.; Song, T.K.; Noh, T.W. Polarization Relaxation Induced by a Depolarization Field in Ultrathin Ferroelectric $BaTiO_3$ Capacitors. *Phys. Rev. Lett.* **2005**, *95*, 237602. [CrossRef] [PubMed]
14. Gao, P.; Zhang, Z.; Li, M.; Ishikawa, R.; Feng, B.; Liu, H.-J.; Huang, Y.-L.; Shibata, N.; Ma, X.; Chen, S.; et al. Possible absence of critical thickness and size effect in ultrathin perovskite ferroelectric films. *Nat. Commun.* **2017**, *8*, 15549. [CrossRef] [PubMed]
15. Highland, M.J.; Fister, T.T.; Richard, M.-I.; Fong, D.D.; Fuoss, P.H.; Thompson, C.; Eastman, J.A.; Streiffer, S.K.; Stephenson, G.B. Polarization Switching without Domain Formation at the Intrinsic Coercive Field in Ultrathin Ferroelectric $PbTiO_3$. *Phys. Rev. Lett.* **2010**, *105*, 167601. [CrossRef] [PubMed]
16. Fong, D.D.; Kolpak, A.M.; Eastman, J.A.; Streiffer, S.K.; Fuoss, P.H.; Stephenson, G.B.; Thompson, C.; Kim, D.M.; Choi, K.J.; Eom, C.B.; et al. Stabilization of Monodomain Polarization in Ultrathin $PbTiO_3$ Films. *Phys. Rev. Lett.* **2006**, *96*, 127601. [CrossRef]
17. Shin, H.W.; Son, J.Y. Imprinted hysteresis loops and size-reduced ferroelectric polarization nanodots in epitaxial $PbTiO_3$ thin film after heat treatment. *Mater. Sci. Eng. B* **2022**, *276*, 115533. [CrossRef]
18. Miao, P.; Zhao, Y.; Luo, N.; Zhao, D.; Chen, A.; Sun, Z.; Guo, M.; Zhu, M.; Zhang, H.; Li, Q. Ferroelectricity and Self-Polarization in Ultrathin Relaxor Ferroelectric Films. *Sci. Rep.* **2016**, *6*, 19965. [CrossRef]
19. Kalinin, S.V.; Kim, Y.; Fong, D.D.; Morozovska, A.N. Surface-screening mechanisms in ferroelectric thin films and their effect on polarization dynamics and domain structures. *Rep. Prog. Phys.* **2018**, *81*, 036502. [CrossRef]
20. Malashevich, A.; Marshall, M.S.J.; Visani, C.; Disa, A.S.; Xu, H.; Walker, F.J.; Ahn, C.H.; Ismail-Beigi, S. Controlling Mobility in Perovskite Oxides by Ferroelectric Modulation of Atomic-Scale Interface Structure. *Nano Lett.* **2018**, *18*, 573–578. [CrossRef]
21. Wojcik, K. Electrical properties of $PbTiO_3$ single crystals doped with lanthanum. *Ferroelectrics* **1989**, *99*, 5–12. [CrossRef]
22. Pan, Z.; Jiang, X.; Chen, J.; Hu, L.; Yamamoto, H.; Zhang, L.; Fan, L.; Fan, X.; Li, Y.-W.; Li, G.; et al. Large spontaneous polarization in polar perovskites of $PbTiO_3$–$Bi(Zn_{\frac{1}{2}}Ti_{\frac{1}{2}})O_3$. *Inorg. Chem. Front.* **2018**, *5*, 1277–1281. [CrossRef]
23. Yan, Y.; Zhou, J.E.; Maurya, D.; Wang, Y.U.; Priya, S. Giant piezoelectric voltage coefficient in grain-oriented modified $PbTiO_3$ material. *Nat. Commun.* **2016**, *7*, 13089. [CrossRef] [PubMed]
24. Sarott, F.; Rossell, M.D.; Fiebig, M.; Trassin, M. Multilevel polarization switching in ferroelectric thin films. *Nat. Commun.* **2022**, *13*, 3159. [CrossRef]
25. Chaupatnaik, A.; Barpanda, P. Perovskite lead-based oxide anodes for rechargeable batteries. *Electrochem. Commun.* **2021**, *127*, 107038. [CrossRef]
26. Szade, J.; Psiuk, B.; Pilch, M.; Waser, R.; Szot, K. Self-neutralization via electroreduction in photoemission from $SrTiO_3$ single crystals. *Appl. Phys. A* **2009**, *97*, 449–454. [CrossRef]
27. Molak, A.; Pawełczyk, M.; Kubacki, J.; Szot, K. Nano-scale chemical and structural segregation induced in surface layer of $NaNbO_3$ crystals with thermal treatment at oxidising conditions studied by XPS, AFM, XRD, and electric properties tests. *Phase Transit.* **2009**, *82*, 662–682. [CrossRef]
28. Bruchhaus, R.; Pitzer, D.; Primig, R.; Schreiter, M.; Wersing, W.; Neumann, N.; Hess, N.; Vollheim, J.; Köhler, R.; Simon, M. A 11 × 6 element pyroelectric detector array utilizing self-polarized PZT thin films grown by sputtering. *Integr. Ferroelectr.* **1997**, *17*, 369–376. [CrossRef]
29. Afanasjev, V.P.; Petrov, A.A.; Pronin, I.P.; Tarakanov, E.A.; Kaptelov, E.J.; Graul, J. Polarization and self-polarization in thin $PbZr_{1\text{-}x}Ti_xO_3$ (PZT) films. *J. Phys. Condens. Matter* **2001**, *13*, 8755. [CrossRef]
30. Pronin, I.P.; Kaptelov, E.Y.; Tarakanov, E.A.; Shaplygina, T.A.; Afanas'ev, V.P.; Pankrashkin, A.V. Self-polarization and migratory polarization in thin lead zirconate-titanate films. *Phys. Solid State* **2002**, *44*, 769–773. translated from *Fiz. Tverd. Tela*, **2002**, *44*, 739. [CrossRef]
31. Lee, J.; Ramesh, R.; Keramidas, V.G.; Warren, W.L.; Pike, G.E.; Evans, J.T. Imprint and oxygen deficiency in $(Pb,La)(Zr,Ti)O_3$ thin-film capacitors with La-Sr-Co-O electrodes. *Appl. Phys. Lett.* **1995**, *66*, 1337–1339. [CrossRef]
32. Szot, K.; Speier, W. Self Polarisation of ABO3 Perowskites (1997–2001). European Patent No. EP0825160, 25 February 1998.
33. Osipov, V.V.; Kiselev, D.A.; Kaptelov, E.Y.; Senkevich, S.V.; Pronin, I.P. Internal field and self-polarization in lead zirconate titanate thin films. *Phys. Solid State* **2015**, *57*, 1793–1799. [CrossRef]
34. Zhong, W.L.; Jiang, B.; Zhang, P.L.; Ma, J.M.; Cheng, H.M.; Yang, Z.H. Phase transition in $PbTiO_3$ ultrafine particles of different sizes. *J. Phys. Condens. Matter* **1993**, *5*, 2619. [CrossRef]
35. Behera, R.K.; Hinojosa, B.B.; Sinnott, S.B.; Asthagiri, A.; Phillpot, S.R. Coupling of surface relaxation and polarization in $PbTiO_3$ from atomistic simulation. *J. Phys. Condens. Matter* **2008**, *20*, 395004. [CrossRef]
36. Fontana, M.D.; Abdi, F.; Wójcik, K. Electro-optical properties of a single domain $PbTiO_3$ crystal. *J. Appl. Phys.* **1995**, *77*, 2102–2106. [CrossRef]
37. Gavrilyachenko, V.G.; Spinko, R.I.; Martynenko, M.A.; Fesenko, E.G. Spontaneous Polarization and Coercive Field of Lead Titanate. *Sov. Phys. Solid State* **1970**, *12*, 1203.
38. Kwapuliński, J.; Kusz, J.; Böhm, H.; Dec, J. Thermal vibrations in $PbTiO_3$ single crystals. *J. Phys. Condens. Matter* **2005**, *17*, 1825–1830. [CrossRef]
39. Cai, M.-Q.; Tang, C.-H.; Tan, X.; Deng, H.-Q.; Hu, W.-Y.; Wang, L.-L.; Wang, Y.-G. First-principles study for the atomic structures and electronic properties of $PbTiO_3$ oxygen-vacancies (001) surface. *Surf. Sci.* **2007**, *601*, 5412–5418. [CrossRef]
40. Szot, K.; Pawelczyk, M.; Herion, J.; Freiburg, C.; Albers, J.; Waser, R.; Hulliger, J.; Kwapulinski, J.; Dec, J. Nature of the surface layer in ABO_3-type perovskites at elevated temperatures. *Appl. Phys. A* **1996**, *62*, 335–343. [CrossRef]

41. Wójcik, K. The influence of point defects on selected properties of $PbTiO_3$ crystals. *Ferroelectrics* **1988**, *82*, 25–35. [CrossRef]
42. Wójcik, K.; Ujma, Z. Nonstoichiometry and optical absorption in $PbZrO_3$ and $PbTiO_3$ single crystals. *Ferroelectrics* **1989**, *89*, 133–142. [CrossRef]
43. Wójcik, K. Wpływ Defektów sieci Krystalicznej na Właściwości Optyczne i Fotoelektryczne Niektórych Materiałów o Strukturze typu Perowskitu. Habilitation Thesis, University of Silesia, Katowice, Poland, 1990. (In Polish)
44. Fesenko, E.G. *Semejstwo Perovskita i Segnetoelektriczestvo (Perovskite Family and Ferroelectricity)*; Atomizdat: Moscow, Russia, 1972.
45. Fridkin, V.M. *Ferroelecrics—Semiconductors*; Chapters 5 and 6; Plenum Publishing Corp: New York, NY, USA, 1980.
46. Jubindo, M.A.P.; Tello, M.J.; Fernandez, J. A new method for measuring the ferroelectric behaviour of crystals at low frequencies. *J. Phys. D Appl. Phys.* **1981**, *14*, 2305. [CrossRef]
47. Wu, Z.; Cohen, R.E. More accurate generalized gradient approximation for solids. *Phys. Rev. B* **2006**, *73*, 235116. [CrossRef]
48. Wortmann, D.; Michalicek, G.; Baadji, N.; Betzinger, M.; Bihlmayer, G.; Bröder, J.; Burnus, T.; Enkovaara, J.; Freimuth, F.; Friedrich, C.; et al. Fleur. Zenodo. 2023. Available online: https://doi.org/10.5281/zenodo.7576163 (accessed on 18 July 2023).
49. Bratkovsky, A.M.; Levanuk, A.P. Continuous Theory of Ferroelectric States in Ultrathin Films with Real Electrodes. *J. Comput. Theor. Nanosci.* **2009**, *6*, 465–489. [CrossRef]
50. Stephanovich, V.A.; Lukyanchuk, I.A.; Karkut, M.G. Domain-Enhanced Interlayer Coupling in Ferroelectric/Paraelectric Superlattices. *Phys. Rev. Lett.* **2005**, *94*, 047601. [CrossRef]
51. Tagantsev, A.K.; Gerra, G. Interface-induced phenomena in polarization response of ferroelectric thin films. *J. Appl. Phys.* **2006**, *100*, 051607. [CrossRef]
52. Lifshitz, E.M.; Pitaevskii, L.P. *Electrodynamics of Continuous Media*; Butterworth-Heinemann: Oxford, UK, 1984.
53. Agranovich, V.M.; Ginzburg, V.L. *Crystal Optics with Spatial Dispersion and Excitons*; Springer: Berlin, Germany, 1984.
54. Steinbach, I. Phase-field models in materials science. *Model. Simul. Mater. Sci. Eng.* **2009**, *17*, 073001. [CrossRef]
55. Kirichenko, E.V.; Stephanovich, V.A. Physical properties of ferroelectric film with continuous space charge distribution. *Phase Transit.* **2014**, *87*, 1165–1173. [CrossRef]
56. Abe, K.; Yanase, N.; Yasumoto, T.; Kawakubo, T. Nonswitching Layer Model for Voltage Shift Phenomena in Heteroepitaxial Barium Titanate Thin Films. *Jpn. J. Appl. Phys.* **2002**, *41*, 6065. [CrossRef]
57. Rolofs, A.; Szot, K.; Waser, R. *Domain Switching and Self-Polarization in Perovskite Thin Films*; Chapter VI in Nanoscale Phenomena in Ferrolectrics Thin Films; Hong, S., Ed.; Kluwer Academic Publishers: Alphen aan den Rijn, The Netherlands, 2004.
58. Fontana, M.; Idrissi, H.; Wojcik, K. Displacive to Order-Disorder Crossover in the Cubic-Tetragonal Phase Transition of $PbTiO_3$. *Europhys. Lett.* **1990**, *11*, 419. [CrossRef]
59. Dai, X.H.; Li, Z.; Xu, X.Z.; Chan, S.-K.; Lam, D.J. Dielectric frequency dispersion behavior in flux grown $PbTiO_3$ single crystals. *Ferroelectrics* **1992**, *135*, 39–48. [CrossRef]
60. Li, Z.; Grimsditch, M.; Foster, C.M.; Chan, S.-K. Dielectric and elastic properties of ferroelectric materials at elevated temperature. *J. Phys. Chem. Solids* **1996**, *57*, 1433–1438. [CrossRef]
61. Kakuta, K.; Tsurumi, T.; Fukunaga, O. Dielectric Property of Flux-Grown $PbTiO_3$ Single Crystal. *Jpn. J. Appl. Phys.* **1995**, *34*, 5341. [CrossRef]
62. He, C.; Wang, Z.; Li, X.; Yang, X.; Long, X.; Ye, Z.-G. Self-polarized high piezoelectricity and its memory effect in ferroelectric single crystals. *Acta Mater.* **2017**, *125*, 498–505. [CrossRef]
63. Bhatti, H.S.; Hussain, S.T.; Khan, F.A.; Hussain, S. Synthesis and induced multiferroicity of perovskite $PbTiO_3$; a review. *Appl. Surf. Sci.* **2016**, *367*, 291–306. [CrossRef]
64. Pressley, L.A.; Sinha, M.; Vivanco, H.K.; Chamorro, J.; Das, S.; Ramesh, R.; McQueen, T.M. Optimization of $PbTiO_3$ Single Crystals with Flux and Laser Floating Zone Method. *Cryst. Growth Des.* **2022**, *22*, 5629–5638. [CrossRef]
65. Bollmann, W.; Wehrhan, G. Lattice disorder and optical absorption of $PbTiO_3$ crystals. *Cryst. Res. Technol.* **1984**, *19*, 85–91. [CrossRef]
66. Dobrikov, A.A.; Presnyakova, O.V.; Zaitsev, V.I.; Prisedskii, V.V.; Pan'ko, G.F. Investigation of $PbTiO_3$ crystal lattice defects by transmission electron microscopy. *Krist. Technik* **1980**, *15*, 207–212. [CrossRef]
67. Prisedskii, W.W.; Komarow, W.P.; Panko, G.F.; Dobrikow, A.A.; Klimow, W.W. Spreaded defects and nonstoichiometry of perovskite-type oxides. *Dokl. A.N. SSSR Chimiia* **1979**, *247*, 620.
68. Prisedsky, V.V.; Pan'ko, G.F.; Klimov, V.V. Linear and planar faults in electron microscopic structures of PZT crystals. *Ferroelectrics* **1985**, *64*, 257–273. [CrossRef]
69. Arredondo, M.; Weyland, M.; Hambe, M.; Ramasse, Q.M.; Munroe, P.; Nagarajan, V. Chemistry of Ruddlesden–Popper Planar Faults at a Ferroelectric–Ferromagnet Perovskite Interface. *J. Appl. Phys.* **2011**, *109*, 084101. [CrossRef]
70. Krakauer, H.; Posternak, M.; Freeman, A.J. Linearized augmented plane-wave method for the electronic band structure of thin films. *Phys. Rev. B* **1979**, *19*, 1706–1719. [CrossRef]
71. Miller, S.L.; Nasby, R.D.; Schwank, J.R.; Rodgers, M.S.; Dressendorfer, P.V. Device modeling of ferroelectric capacitors. *J. Appl. Phys.* **1990**, *68*, 6463–6471. [CrossRef]
72. Ujma, Z.; Handerek, J. The influence of defects in the Pb and O sub-lattices on dielectric properties and phase transitions in $PbZrO_3$. *J. Phase Transit.* **1983**, *3*, 121–130. [CrossRef]
73. Ujma, Z.; Hańderek, J. The pyroelectric effect in single crystal and ceramic $PbZrO_3$. *Ferroelectrics* **1981**, *33*, 37–42. [CrossRef]
74. Ujma, Z.; Hańderek, J. Space-charge polarization and phase transitions in lead zirconate. *Phase Transit.* **1980**, *1*, 363–376. [CrossRef]

75. Kobayashi, Y.; Egawa, T.; Tamura, S.; Imanaka, N.; Adach, G.-Y. Trivalent Al^{3+} Ion Conduction in Aluminum Tungstate Solid. *Chem. Mater.* **1997**, *9*, 1649–1654. [CrossRef]
76. Imanaka, N.; Kobayashi, Y.; Fujiwara, K.; Asano, T.; Okazaki, Y.; Adach, G.-Y. Trivalent Rare Earth Ion Conduction in the Rare Earth Tungstates with the $Sc_2(WO_4)_3$-Type Structure. *Chem. Mater.* **1998**, *10*, 2006–2012. [CrossRef]
77. Thangadurai, V.; Weppner, W. Determination of the Sodium Ion Transference Number of the Dion-Jacobson Type Layered Perovskite $NaCa_2Nb_3O_{10}$ Using AC Impedance and DC Methods. *Chem. Mater.* **2002**, *14*, 1136–1143. [CrossRef]
78. Ahn, C.H.; Rabe, K.M.; Triscone, J.-M. Ferroelectricity at the nanoscale: Local polarization in oxide thin films and heterostructures. *Science* **2004**, *303*, 488–491. [CrossRef]
79. Morozovska, A.N.; Eliseev, E.A.; Glinchuk, M.D. Size effects and depolarization field influence on the phase diagrams of cylindrical ferroelectric nanoparticles. *Physica B* **2007**, *387*, 358–366. [CrossRef]
80. Kubacki, J.; Molak, A.; Rogala, M.; Rodenbücher, C.; Szot, K. Metal–insulator transition induced by non-stoichiometry of surface layer and molecular reactions on single crystal $KTaO_3$. *Surf. Sci.* **2012**, *606*, 1252–1262. [CrossRef]
81. Garrity, K.; Kakekhani, A.; Kolpak, A.; Ismail-Beigi, S. Ferroelectric surface chemistry: First-principles study of the $PbTiO_3$ surface. *Phys. Rev. B* **2013**, *88*, 045401. [CrossRef]
82. Bennett, J.W.; Grinberg, I.; Rappe, A.M. New Highly Polar Semiconductor Ferroelectrics through d^8 Cation-O Vacancy Substitution into $PbTiO_3$: A Theoretical Study. *J. Am. Chem. Soc.* **2008**, *130*, 17409–17412. [CrossRef] [PubMed]
83. Genenko, Y.A. Space-charge mechanism of aging in ferroelectrics: An analytically solvable two-dimensional model. *Phys. Rev. B* **2008**, *78*, 214103. [CrossRef]
84. Zimmer, M.; Junquera, J.; Ghosez, P. Fundamental Physics of Ferroelectrics. In Proceedings of the AIP Conference Proceedings, Washington, DC, USA, 3–6 February 2002; Cohen, R.E., Ed.; AIP: College Park, MD, USA, 2002; Volume 626, p. 232.
85. Ghosez, P.; Michenaud, J.P.; Gonze, X. Dynamical atomic charges: The case of ABO_3 compounds. *Phys. Rev. B* **1998**, *58*, 6224–6240. [CrossRef]
86. Kobertz, D.; Müller, M.; Molak, A. Vaporization and Caloric Studies on Lead Titanate. *Calphad* **2014**, *46*, 62–79. [CrossRef]